

Conditional PED-ANOVA: Hyperparameter Importance in Hierarchical & Dynamic Search Spaces

Kaito Baba

Preferred Networks, Inc.
Tokyo, Japan
k.ai.to47802@gmail.com

Yoshihiko Ozaki

Preferred Networks, Inc.
Tokyo, Japan
yozaki@preferred.jp

Shuhei Watanabe*

SB Intuitions Corp.
Tokyo, Japan
shuhei.watanabe@sbintuitions.co.jp

Abstract

We propose *conditional PED-ANOVA* (*condPED-ANOVA*), a principled framework for estimating hyperparameter importance (HPI) in conditional search spaces, where the presence or domain of a hyperparameter can depend on other hyperparameters. Although the original PED-ANOVA provides a fast and efficient way to estimate HPI within the top-performing regions of the search space, it assumes a fixed, unconditional search space and therefore cannot properly handle conditional hyperparameters. To address this, we introduce a conditional HPI for top-performing regions and derive a closed-form estimator that accurately reflects conditional activation and domain changes. Experiments show that naive adaptations of existing HPI estimators yield misleading or uninterpretable importance estimates in conditional settings, whereas *condPED-ANOVA* consistently provides meaningful importances that reflect the underlying conditional structure.

CCS Concepts

- Computing methodologies → Machine learning approaches;
- Mathematics of computing → Mathematical analysis.

Keywords

Analysis of Variance, Hyperparameter Importance, Conditional Search Space, Automated Machine Learning

1 Introduction

Analysis of parameter importance [14, 15, 35, 36] is a central tool for understanding and designing optimization procedures. Over the past decade, techniques for measuring the importance of parameters have attracted considerable attention in the automated machine learning (AutoML) community [5, 16, 41], particularly for improving the efficiency of hyperparameter optimization (HPO) [2, 3, 22, 34]. Given a hyperparameter search space and a set of evaluated configurations, methods for hyperparameter importance (or HPI methods for short) aim to quantify how strongly each hyperparameter influences the observed performance. Such information is useful for interpreting optimization runs, identifying critical design choices, detecting irrelevant or redundant parameters, and guiding subsequent search or manual tuning [13, 27]. As a result, HPI is widely used across various settings, including HPO of machine learning models and HPO algorithm design, where understanding hyperparameter sensitivity is often essential [29, 39, 41, 44].

Classic HPI methods such as functional analysis of variance (f-ANOVA) [16] quantify HPI by measuring how much variance in

the objective can be attributed to each hyperparameter. However, their existing local variants mix contributions from unpromising regions, leading to inaccurate estimates of HPI in top-performing subspaces [6, 16]. PED-ANOVA [42] mitigates this by defining local HPI within a top-performing subset of the search space and efficiently approximating it using the Pearson divergence between one-dimensional distributions of each hyperparameter. Moreover, PED-ANOVA computes both global and local HPIs substantially faster than f-ANOVA while maintaining accurate HPI estimates. Thanks to this combination of speed and reliability, it has been adopted for HPI analysis in practical HPO frameworks, such as Optuna [1], demonstrating its utility in real-world workflows.

However, we argue that PED-ANOVA has a practical limitation: it cannot properly handle *hierarchical/dynamic* search spaces, where the presence/domain of a hyperparameter depends on other hyperparameters (hereafter referred to as *conditional* search spaces). In practice, many real-world problems involve such conditional search spaces [18]. Typical examples include model selection, where hyperparameters are dependent on a chosen algorithm [8, 12, 20, 40], and neural network architecture design, where active parameters depend on the chosen layers [4, 38]. Unfortunately, PED-ANOVA cannot be directly applied to such settings, since it assumes a fixed, unconditional search space and defines distributions over a single, fixed domain for each hyperparameter. We observe that naive extensions of PED-ANOVA, such as filtering inactive configurations, imputing missing values, or artificially expanding parameter domains, do not resolve this issue: these heuristics often violate the conditional semantics of the search space and yield unnatural or uninterpretable HPI estimates (cf. Section 5.4).

To address this limitation, we propose *conditional PED-ANOVA* (*condPED-ANOVA*), a principled framework for estimating HPI in conditional search spaces. We identify a critical flaw in the original definition of local HPI in PED-ANOVA when applied to conditional search spaces: the importance of hyperparameters that induce conditionality is spuriously attributed to the hyperparameters whose domains or activation depend on them, leading to systematically misleading importance estimates. Consequently, merely constructing a method that correctly computes local HPI in conditional search spaces is still insufficient. We introduce *conditional local HPI*, which measures importance within top-performing regions without confounding from conditional activation or domain changes. Building on this definition, we derive a closed-form PED-ANOVA-style estimator that remains efficient and yields an interpretable HPI in conditional settings. Experiments confirm that *condPED-ANOVA* reliably produces a meaningful HPI that reflects the underlying conditional structure, while naive extensions of existing methods fail to do so.

*The work was conducted while Shuhei Watanabe was affiliated with Preferred Networks, Inc.

Our contributions are summarized as follows:

- We identify a fundamental pitfall of original local HPI in conditional search spaces: the contribution of conditioning hyperparameters is spuriously attributed to conditionally active (or domain-shifted) hyperparameters, yielding misleading importance estimates.
- We introduce *conditional local HPI*, a definition that measures importance within top-performing regions while accounting for conditional activation and domain changes.
- We derive a closed-form PED-ANOVA-style estimator for conditional local HPI, retaining the efficiency of the original PED-ANOVA via Pearson divergence of one-dimensional distributions estimated with KDE.
- We empirically demonstrate that condPED-ANOVA consistently produces meaningful importances in conditional settings, whereas naive extensions of existing methods, including PED-ANOVA, produce unnatural results.

2 Related Work

Here, we review prior work most relevant to ours. Additional related work is provided in Appendix A.

2.1 Variance-Based HPI and f-ANOVA

HPI aims to quantify how strongly each hyperparameter (and their interactions) influences performance, typically to support search-space design, debugging, and interpretation of HPO runs. Early work on parameter importance analysis builds on variance-based sensitivity analysis such as Sobol indices [35, 36] and ANOVA decompositions [14, 15], which attribute the global variance of an objective to individual coordinates and their interactions. In the context of HPO, f-ANOVA [16] applies this idea to HPO objectives by fitting a surrogate model such as a random forest over the hyperparameter space and then estimating main and interaction effects by Monte Carlo integration over the surrogate. This yields importance values that reflect how much of the global variation in performance across the entire search space can be explained by each hyperparameter. f-ANOVA includes efficient marginal computation over random-forest predictions and produces a global ranking of important hyperparameters, making it a standard post-hoc analysis tool in AutoML and algorithm configuration.

2.2 PED-ANOVA

PED-ANOVA [42] extends HPI to settings where the region of interest is not an entire search space. It defines local HPI as the variance contribution of each hyperparameter within the top- γ subset of the search space, thereby measuring importance directly in the most relevant region. It further shows that this local HPI can be approximated in closed form using the Pearson divergence between the one-dimensional distributions of each hyperparameter of two top-performing subsets, estimated via one-dimensional KDEs. Empirically, this leads to much faster HPI computation than f-ANOVA while maintaining accurate importance estimates in top-performing subspaces. The details of PED-ANOVA are reviewed in Section 3.

Our approach follows a PED-ANOVA-style framework, while enabling effective HPI estimation in conditional search spaces that arise in many real-world problem settings.

2.3 Conditional Hyperparameters in HPO

Many HPO algorithms furthermore operate on conditional search spaces, where certain hyperparameters are active only under specific parent choices, and their domains may also change depending on those choices (e.g., algorithm selection or internal mode switches). This view is made explicit in practical AutoML systems, such as Auto-WEKA [40], auto-sklearn [11, 12], which describe conditional hyperparameters that are only relevant when a parent hyperparameter takes a particular value. Among widely used optimizers, SMAC [22] is designed to handle such conditional hierarchies in CASH-style spaces [40], while TPE [2] formulates the search space as a tree-structured generative process where some variables are only well-defined under specific upstream choices. BOHB [9] combines Hyperband [21] with a Bayesian-optimization component built on TPE, thereby optimizing over the same tree-structured conditional spaces while exploiting cheap low-fidelity evaluations. Beyond these algorithms, a complementary line of work develops BO surrogates tailored to conditional domains to better share information across branches [19, 26, 38].

2.4 HPI under Conditional Search Spaces

In conditional search spaces, applying standard HPI pipelines generally requires mapping configurations to a fixed representation, typically by imputing inactive hyperparameters with default values as done in SMAC-style toolchains and related preprocessing workflows [22]. Practical analysis suites such as CAVE [6] (and its integration in BOAH [23]) then compute importance post-hoc using methods like f-ANOVA and local parameter importance, including for multi-fidelity runs. Optuna’s importance API highlights a common limitation of conditional spaces: by default, it evaluates only parameters that appear and have the same domain in all samples, excluding conditional parameters [1]. Recent work on multi-objective HPI likewise treats missing values arising from conditional hyperparameters in preprocessing before applying surrogate-based importance measures such as f-ANOVA and ablation paths [39].

Consequently, despite the fact that conditional hyperparameters arise frequently in practical HPO settings, prior HPI methods have lacked a principled way to handle conditional hyperparameters directly, without resorting to default-value imputation or discarding them during preprocessing. This limitation has prevented existing approaches from faithfully capturing the importance of hyperparameters within the conditional structure of the search space.

3 Preliminaries

3.1 Notations

Let $\mathcal{X} := \mathcal{X}^{(1)} \times \dots \times \mathcal{X}^{(D)}$ be the D -dimensional search space for hyperparameters $\mathbf{x} := (x^{(1)}, \dots, x^{(D)}) \in \mathcal{X}$. Let $f: \mathcal{X} \rightarrow \mathbb{R}$ be an objective function to be minimized. We observe a finite evaluation set $\{(\mathbf{x}_n, f(\mathbf{x}_n))\}_{n=1}^N$, where each \mathbf{x}_n is sampled from a distribution $p_0(\mathbf{x})$. For $\gamma \in (0, 1]$, let $f_\gamma \in \mathbb{R}$ denote the lower (i.e., better) empirical γ -quantile of the observed values, i.e., f_γ satisfies $\#\{n \mid f(\mathbf{x}_n) \leq f_\gamma\} = \lfloor \gamma N \rfloor$. The corresponding top- γ set is represented as $\mathcal{X}_\gamma := \{\mathbf{x} \in \mathcal{X} \mid f(\mathbf{x}) \leq f_\gamma\}$.

3.2 Local HPI

To quantify how strongly the d -th hyperparameter influences the performance in the top- γ set, a local HPI based on a local marginal variance is introduced [42]. Let $b_\gamma(\mathbf{x}) := \mathbf{1}\{\mathbf{x} \in \mathcal{X}_\gamma\} = \mathbf{1}\{f(\mathbf{x}) \leq f_\gamma\}$ be the indicator function of whether hyperparameters \mathbf{x} belong to the top- γ performers. The *local mean* m_γ of the objective and the *local marginal mean* $f_\gamma^{(d)}(\mathbf{x}^{(d)})$ for the d -th hyperparameter $\mathbf{x}^{(d)}$ at level γ are defined as:

$$m_\gamma := \mathbb{E}_{\mathbf{x} \sim p_0}[f(\mathbf{x}) | b_\gamma(\mathbf{x})] = \frac{\mathbb{E}_{\mathbf{x} \sim p_0}[f(\mathbf{x}) b_\gamma(\mathbf{x})]}{\mathbb{E}_{\mathbf{x} \sim p_0}[b_\gamma(\mathbf{x})]},$$

$$f_\gamma^{(d)}(\mathbf{x}^{(d)}) := \mathbb{E}_{\mathbf{x}^{(d)} \sim p_0^{(d)}}[f(\mathbf{x}) | b_\gamma(\mathbf{x}), \mathbf{x}^{(d)}]$$

$$= \frac{\mathbb{E}_{\mathbf{x}^{(d)} \sim p_0^{(d)}}[f(\mathbf{x}) b_\gamma(\mathbf{x}) | \mathbf{x}^{(d)}]}{\mathbb{E}_{\mathbf{x}^{(d)} \sim p_0^{(d)}}[b_\gamma(\mathbf{x}) | \mathbf{x}^{(d)}]},$$

where $\mathbf{x}^{(\bar{d})} := (x^{(1)}, \dots, x^{(d-1)}, x^{(d+1)}, \dots, x^{(D)})$ denotes all hyperparameters except for the d -th one. The local marginal mean $f_\gamma^{(d)}(\mathbf{x}^{(d)})$ is obtained by taking the mean over all hyperparameters $\mathbf{x}^{(\bar{d})}$ within the top- γ region while keeping the d -th hyperparameter fixed at $\mathbf{x}^{(d)}$, in a manner similar to marginalization.

The *local marginal variance* for the d -th hyperparameter at level γ is then defined as follows:

$$v_\gamma^{(d)} := \text{Var}_{\mathbf{x} \sim p_0}(f_\gamma^{(d)}(\mathbf{x}^{(d)}) | b_\gamma(\mathbf{x}))$$

$$= \frac{\mathbb{E}_{\mathbf{x} \sim p_0}[(f_\gamma^{(d)}(\mathbf{x}^{(d)}) - m_\gamma)^2 b_\gamma(\mathbf{x})]}{\mathbb{E}_{\mathbf{x} \sim p_0}[b_\gamma(\mathbf{x})]}.$$

Using this quantity, the *local HPI* for the d -th hyperparameter at level γ is then defined as its normalized form:

$$\text{Local HPI} := v_\gamma^{(d)} / \sum_{d'=1}^D v_\gamma^{(d')}.$$

3.3 PED-ANOVA

PED-ANOVA [42] introduces an efficient approximation of the local HPI of the objective f by computing the local HPI of a tighter level-set indicator function $b_{\gamma'}(\mathbf{x}) := \mathbf{1}\{\mathbf{x} \in \mathcal{X}_{\gamma'}\}$, where $0 < \gamma' < \gamma$. A key result in PED-ANOVA shows that the local marginal variance for $b_{\gamma'}$ admits the following closed-form expression:

$$v_\gamma^{(d)} = \left(\frac{\gamma'}{\gamma} \right)^2 D_{\text{PE}} \left(p_{\gamma'}^{(d)} \parallel p_\gamma^{(d)} \right), \quad (1)$$

where $p_\gamma^{(d)}$ and $p_{\gamma'}^{(d)}$ are the empirical one-dimensional probability density functions (PDFs) of the d -th hyperparameter induced by the samples in the top- γ and top- γ' subsets, respectively. In practice, the PDFs are estimated via KDE using the observed samples. Here, $D_{\text{PE}}(p \parallel q)$ denotes the Pearson (χ^2) divergence between two PDFs p and q , defined as:

$$D_{\text{PE}}(p \parallel q) := \int \left(\frac{p(x)}{q(x)} - 1 \right)^2 q(x) dx.$$

Note that this divergence is well-defined in the present setting, since $\mathcal{X}_{\gamma'} \subset \mathcal{X}_\gamma$ implies that the density $p_{\gamma'}^{(d)}$ has support only where $p_\gamma^{(d)}$ is nonzero, so the ratio $p_{\gamma'}^{(d)} / p_\gamma^{(d)}$ is well-defined.

PED-ANOVA uses this closed-form expression to compute the local HPI solely from one-dimensional PDFs. In the original PED-ANOVA experiments, this approach was shown to yield dramatically faster HPI calculation compared to f-ANOVA, while maintaining comparable quality in the resulting importance measures.

4 condPED-ANOVA: Hyperparameter Importance in Conditional Search Spaces

In this section, we present condPED-ANOVA, a principled approach for efficient HPI computation in conditional search spaces. Rigorous details are provided in Appendix B.

4.1 Regime-Based Representation of Conditional Hyperparameters

In practice, many hyperparameters are conditional: the presence of a hyperparameter and its domain can change depending on other hyperparameters [4, 8, 12, 18, 20, 38, 40].

We now formalize such behavior. To handle such conditional structure, we partition the behavior of the d -th hyperparameter into a finite number of *regimes*. Each regime $i^{(d)} \in \{1, \dots, K^{(d)}\}$ has its own domain $\mathcal{Z}_i^{(d)}$ for $x^{(d)}$, which may differ across regimes. When $x^{(d)}$ is inactive in regime $i^{(d)}$, we represent this by a special symbol \perp and set $\mathcal{Z}_i^{(d)} = \{\perp\}$; otherwise, $\mathcal{Z}_i^{(d)}$ is the usual domain (e.g., an interval or a discrete set), whose range may depend on $i^{(d)}$.

For example, suppose $x^{(0)}$ selects a learning algorithm, such as a neural network or a tree-based model. If $x^{(0)} = \text{neural}$, $x^{(1)}$ may correspond to the number of layers with domain $\mathcal{Z}_{\text{neural}}^{(1)} = \{1, \dots, L_{\max}\}$, while $x^{(2)}$ is inactive, i.e., $\mathcal{Z}_{\text{neural}}^{(2)} = \{\perp\}$. Conversely, if $x^{(0)} = \text{tree}$, $x^{(1)}$ is inactive, i.e., $\mathcal{Z}_{\text{tree}}^{(1)} = \{\perp\}$, and $x^{(2)}$ may represent the minimum split gain with domain $\mathcal{Z}_{\text{tree}}^{(2)} = \mathbb{R}_+$. Here, the choice of $x^{(0)}$ induces regimes $i^{(d)} \in \{\text{neural, tree}\}$ under which $x^{(1)}$ and $x^{(2)}$ have regime-specific domains or become inactive.

4.2 Conditional Local HPI via Within-Regime Variance

Let $I^{(d)}$ and $Z^{(d)}$ denote random variables taking values in $\{1, \dots, K^{(d)}\}$ and $\mathcal{Z}_{I^{(d)}}^{(d)}$, respectively. We write the local marginal mean $f_\gamma^{(d)}(\mathbf{x}^{(d)})$ as $g_\gamma^{(d)}(I^{(d)}, Z^{(d)})$.

We observe that the standard local HPI based on the local marginal variance $v_\gamma^{(d)}$ mixes two distinct sources of variation: differences *within* each regime and differences *between* (inter) regimes. This can be seen through the following variance decomposition:

$$v_\gamma^{(d)} = \text{Var}_{I^{(d)}, Z^{(d)}} \left(g_\gamma^{(d)}(I^{(d)}, Z^{(d)}) \right)$$

$$= \underbrace{\mathbb{E}_{I^{(d)}} \left[\text{Var}_{Z^{(d)}} \left(g_\gamma^{(d)}(I^{(d)}, Z^{(d)}) \mid I^{(d)} \right) \right]}_{\text{within-regime variance}}$$

$$+ \underbrace{\text{Var}_{I^{(d)}} \left(\mathbb{E}_{Z^{(d)}} \left[g_\gamma^{(d)}(I^{(d)}, Z^{(d)}) \mid I^{(d)} \right] \right)}_{\text{inter-regime variance}}, \quad (2)$$

where the expectations and variances are taken under the empirical distribution restricted to the top- γ region \mathcal{X}_γ .

Algorithm 1 condPED-ANOVA Computation for the d -th Hyperparameter

Input: Evaluation set $\mathcal{D} = \{(\mathbf{x}_n, f(\mathbf{x}_n))\}_{n=1}^N$, hyperparameter index d , quantile levels $0 < \gamma' \leq \gamma \leq 1$

Output: The within-regime local marginal variance $v_{\gamma, \text{within}}^{(d)}$ for the d -th hyperparameter $x^{(d)}$

- 1: Compute empirical γ' - and γ - quantiles $f_{\gamma'}$ and f_{γ} of $\{f(\mathbf{x}_n)\}_{n=1}^N$
- 2: Define top-performing subsets: $\mathcal{D}_{\gamma'} \leftarrow \{(\mathbf{x}_n, f(\mathbf{x}_n)) \mid f(\mathbf{x}_n) \leq f_{\gamma'}\}$, $\mathcal{D}_{\gamma} \leftarrow \{(\mathbf{x}_n, f(\mathbf{x}_n)) \mid f(\mathbf{x}_n) \leq f_{\gamma}\}$
- 3: **for** $i = 1, \dots, K^{(d)}$ **do** ▷ process each regime i
- 4: $\mathcal{D}_{\gamma', i}^{(d)}, \mathcal{D}_{\gamma, i}^{(d)} \leftarrow$ Extract samples in regime i from $\mathcal{D}_{\gamma'}$ and \mathcal{D}_{γ}
- 5: $p_{\gamma', i}^{(d)}, p_{\gamma, i}^{(d)} \leftarrow$ Estimate via one-dimensional KDE from the samples $\mathcal{D}_{\gamma', i}^{(d)}$ and $\mathcal{D}_{\gamma, i}^{(d)}$
- 6: $L_i^{\text{within}} \leftarrow D_{\text{PE}}\left(p_{\gamma', i}^{(d)} \parallel p_{\gamma, i}^{(d)}\right)$ ▷ within-regime Pearson divergence
- 7: $\alpha_i^{(d)} \leftarrow |\mathcal{D}_{\gamma', i}| / |\mathcal{D}_{\gamma'}|$, $\beta_i^{(d)} \leftarrow |\mathcal{D}_{\gamma, i}| / |\mathcal{D}_{\gamma}|$ ▷ regime probabilities in top γ' and γ subsets
- 8: **end for**
- 9: **return** $\left(\frac{\gamma'}{\gamma}\right)^2 \sum_{i=1}^{K^{(d)}} \frac{(\alpha_i^{(d)})^2}{\beta_i^{(d)}} L_i^{\text{within}}$ ▷ weighted aggregation of within-regime divergences

The inter-regime variance captures differences across regimes, weighted by their frequency in the top- γ region. However, for conditional hyperparameters, the regime $I^{(d)}$ is determined by other hyperparameters (e.g., parent choices) rather than by the d -th hyperparameter itself. As a result, attributing this inter-regime effect to the d -th hyperparameter is often inappropriate: it can reflect changes in upstream decisions rather than the effect of the value of $x^{(d)}$ itself. In fact, we can show that the standard local marginal variance of a conditioned hyperparameter includes the conditioning variable's local marginal variance, and is therefore always no smaller than it (cf. Theorem E.1 in Appendix E.1). In particular, this leakage implies that even inactive hyperparameters can be assigned non-negligible importance solely due to upstream choices. Such behavior is undesirable because tuning an inactive hyperparameter has no effect on the objective and is therefore meaningless.

Motivated by this consideration, we define the local HPI for conditional hyperparameters using only the within-regime component:

Definition 4.1 (Conditional Local HPI). For a conditional hyperparameter $x^{(d)}$, we define the *conditional local HPI* at level γ as:

$$\text{Conditional Local HPI} := v_{\gamma, \text{within}}^{(d)} / \sum_{d'=1}^D v_{\gamma, \text{within}}^{(d')}, \quad (3)$$

where $v_{\gamma, \text{within}}^{(d)}$ is the within-regime local marginal variance defined as:

$$v_{\gamma, \text{within}}^{(d)} := \mathbb{E}_{I^{(d)}} \left[\text{Var}_{Z^{(d)}} \left(g_{\gamma}^{(d)}(I^{(d)}, Z^{(d)}) \mid I^{(d)} \right) \right]. \quad (4)$$

Intuitively, $v_{\gamma, \text{within}}^{(d)}$ quantifies how much the value of the d -th hyperparameter changes the likelihood of being in the tighter top set $X_{\gamma'}$, *after fixing the regime*. When the hyperparameter is not conditional (i.e., $K^{(d)} = 1$), the inter-regime term in Equation (2) vanishes and $v_{\gamma, \text{within}}^{(d)}$ reduces to the standard local HPI. The empirical difference in HPI performance between $v_{\gamma, \text{within}}^{(d)}$ and the original $v_{\gamma}^{(d)}$ is examined in detail in Section 5.5.

4.3 condPED-ANOVA

We now derive a closed-form condPED-ANOVA estimator that efficiently computes the within-regime local marginal variance of each

hyperparameter from one-dimensional PDFs within each regime. The conditional local HPI then follows immediately by normalization, as defined in Equation (3). The pseudocode is provided in Algorithm 1.

For the d -th hyperparameter, let $\mathcal{D}_{\gamma'} := \{(\mathbf{x}_n, f(\mathbf{x}_n)) \mid f(\mathbf{x}_n) \leq f_{\gamma'}\}$ and $\mathcal{D}_{\gamma} := \{(\mathbf{x}_n, f(\mathbf{x}_n)) \mid f(\mathbf{x}_n) \leq f_{\gamma}\}$ denote the top- γ' and top- γ evaluation subsets, respectively. For each regime $i^{(d)} \in \{1, \dots, K^{(d)}\}$, let $\mathcal{D}_{\gamma', i}^{(d)}$ and $\mathcal{D}_{\gamma, i}^{(d)}$ be the samples in regime $i^{(d)}$ within $\mathcal{D}_{\gamma'}$ and \mathcal{D}_{γ} , respectively. We define the regime probabilities:

$$\alpha_i^{(d)} := \frac{|\mathcal{D}_{\gamma', i}^{(d)}|}{|\mathcal{D}_{\gamma'}|}, \quad \text{and} \quad \beta_i^{(d)} := \frac{|\mathcal{D}_{\gamma, i}^{(d)}|}{|\mathcal{D}_{\gamma}|}.$$

For each regime $i^{(d)}$, let $p_{\gamma', i}^{(d)}$ and $p_{\gamma, i}^{(d)}$ denote the one-dimensional PDFs of the d -th hyperparameter. In practice, these PDFs are estimated using KDE from the samples in $\mathcal{D}_{\gamma', i}^{(d)}$ and $\mathcal{D}_{\gamma, i}^{(d)}$, respectively.

With these definitions, we obtain the following closed-form expression for the within-regime local marginal variance:

THEOREM 4.2 (CONDPED-ANOVA). Let $0 < \gamma' < \gamma \leq 1$. The within-regime local marginal variance for the d -th hyperparameter at level γ , computed using the indicator function $b_{\gamma'} := \mathbf{1}\{x \in X_{\gamma'}\}$, is given by:

$$v_{\gamma, \text{within}}^{(d)} = \left(\frac{\gamma'}{\gamma}\right)^2 \sum_{i=1}^{K^{(d)}} \frac{(\alpha_i^{(d)})^2}{\beta_i^{(d)}} D_{\text{PE}}\left(p_{\gamma', i}^{(d)} \parallel p_{\gamma, i}^{(d)}\right). \quad (5)$$

By normalizing the variance across all hyperparameters as defined in Equation (3), we obtain the conditional local HPI for the d -th hyperparameter.

The proof of Theorem 4.2 is provided in Appendix B. Equation (5) aggregates within-regime distributional changes using regime-dependent weights $(\alpha_i^{(d)})^2 / \beta_i^{(d)}$. Intuitively, this weighting emphasizes regimes that are enriched in the tighter top set (i.e., with larger $(\alpha_i^{(d)})^2 / \beta_i^{(d)}$), while attributing importance only to changes *within* each regime. If a regime corresponds to an inactive configuration (so the value is always \perp), then $p_{\gamma', i}^{(d)}$ and $p_{\gamma, i}^{(d)}$ are degenerate at \perp and the corresponding divergence is zero. When the hyperparameter is not conditional, we have $K^{(d)} = 1$ and $\alpha_1^{(d)} = \beta_1^{(d)} = 1$, so Equation (5) reduces to the original PED-ANOVA in Equation (1).

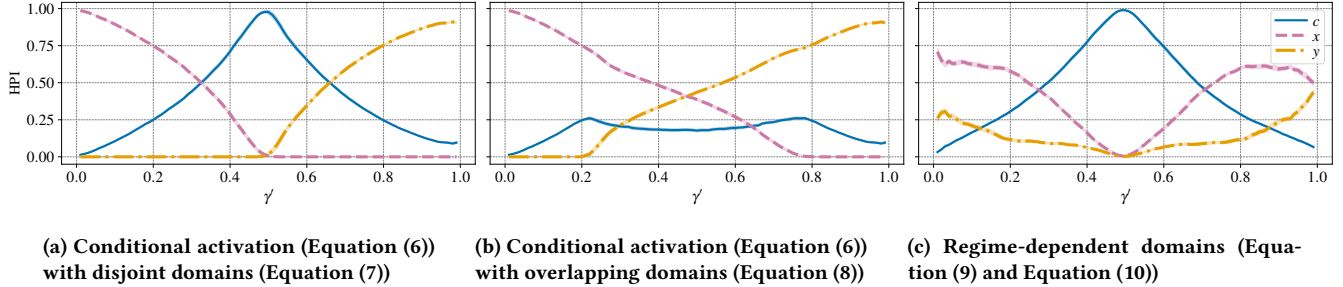


Figure 1: condPED-ANOVA ($\gamma = 1.0$) HPI computed for the synthetic objectives. For the objective with conditional activation (Equation (6)), the gating hyperparameter c determines which branch is active: x is present only when $c < 0.5$, whereas y is present only when $c \geq 0.5$. For the objective with regime-dependent domains (Equation (9)), the gating hyperparameter c determines the domain of x and y . The lines denote the mean, and the shaded regions denote the standard error, both computed over ten independent runs with different random seeds. The results on other values of γ are provided in Figure 5.

5 Numerical Experiments

Here, we first empirically validate condPED-ANOVA on synthetic problems to verify that it properly reflects conditional structure, including parameter activation and regime-dependent domains. We choose a synthetic setting because the expected behavior is clear and easy to diagnose, unlike real-world objectives where the “correct” importance patterns are often ambiguous. Further experimental results, such as runtime comparison, are available in Appendix C.

5.1 Common Experimental Setup

We use a fixed evaluation budget of $N = 1,000$ and draw each sample independently from a uniform distribution over the search space. We consider three choices of $\gamma \in \{1.0, 0.75, 0.5\}$. For each choice of γ , we sweep γ' from 0.01 up to $\gamma - 0.01$ in increments of 0.01, and run experiments for all resulting (γ', γ) quantile pairs. Our condPED-ANOVA implementation is built on top of the PED-ANOVA implementation in Optuna [1]. We repeat the HPI computation with 10 different random seeds and report the mean and the standard error across runs. Further details are provided in Appendix D.1.

5.2 Conditional Activation (Presence/Absence)

5.2.1 Problem Setting. We first consider a simple synthetic optimization problem with a conditional search space, where the active variable switches depending on a gating parameter. The objective function is defined as:

$$f(c, x, y) = \begin{cases} x, & \text{if } c < 0.5, \\ y, & \text{if } c \geq 0.5, \end{cases} \quad \text{with } c \in [0, 1]. \quad (6)$$

Our goal is to minimize f . Here, only one of (x, y) is active depending on the value of c . That is, when $c < 0.5$, the parameter x is active and y is inactive; when $c \geq 0.5$, vice versa.

We study the following two domain settings:

$$(\text{Disjoint domains}) \quad x \in [-5, -2], y \in [2, 5], \quad (7)$$

$$(\text{Overlapping domains}) \quad x \in [-5, 2], y \in [-2, 5]. \quad (8)$$

The first setting creates a clear separation between the two branches, whereas the second introduces overlap between the active-variable

ranges, making the conditional structure less trivially identifiable from the returned objective values.

5.2.2 Results and Discussion. The results are shown in Figures 1a and 1b. The value at each γ' can be interpreted as a *target-dependent* importance: it indicates which hyperparameters matter most if we aim to optimize the objective up to the top- γ' performance.

We first discuss the disjoint-domain setting (Equation (7)) with $\gamma = 1.0$ (Figure 1a). In this figure, around $\gamma' \approx 0.5$, the HPI of the gating variable c is the largest, whereas for a tighter target such as $\gamma' \approx 0.1$, the HPI shifts to x , and for looser targets such as $\gamma' \approx 0.9$, the HPI is dominated by y . This behavior is intuitive. When $c < 0.5$, the objective equals x and is restricted to a low-valued range (i.e., better performance), while when $c \geq 0.5$, the objective equals y and lies in a high-valued range (i.e., worse performance). Accordingly, whether a sample achieves at least median-level performance is largely determined by which branch is selected, which is reflected by the high importance of c around $\gamma' \approx 0.5$. On the other hand, to achieve further better performance (smaller γ'), it is no longer sufficient to select the favorable branch; one must further optimize the active variable itself, which explains the increasing importance of x as γ' decreases. Moreover, for $\gamma' < 0.5$, top- γ' performance requires the $c < 0.5$ branch and y to be inactive, which is consistent with the (near) zero importance of y . Conversely, for $\gamma' > 0.5$, whether a sample falls into the top- γ' region is determined by selecting the $c \geq 0.5$ branch, leading x to be inactive and unimportant.

We next discuss the overlapping-domain setting (Equation (8)) with $\gamma = 1.0$ (Figure 1b). In this setting, the domains of x and y overlap, so the objective values are no longer cleanly separated by the gating variable c alone. Consequently, around $\gamma' \approx 0.5$ the HPI of c is no longer close to one, and both x and y also exhibit non-negligible importance. As γ' decreases, the contribution of y persists up to approximately $\gamma' \approx 0.2$, which corresponds to the best values attainable by the y -branch (near $y = -2$). For tighter targets beyond this point, achieving top- γ' performance requires selecting the $c < 0.5$ branch, consistent with the importance of y dropping to (near) zero. Within the $c < 0.5$ branch, achieving higher performance increasingly depends on the precise value of x , which explains why the HPI of x grows as γ' becomes smaller.

Also, under both domain settings, the resulting HPI is approximately symmetric for $\gamma' < 0.5$ and $\gamma' > 0.5$, reflecting that the objective function is symmetric between the top and bottom regions. However, in the region $\gamma' > 0.5$, changing c can still improve the objective value; consequently, a small but non-zero importance for c remains even around $\gamma' \approx 0.0$, leading to a slight asymmetry. This asymmetry arises from the fact that we minimize the objective, which breaks the top–bottom symmetry.

These results suggest that condPED-ANOVA yields sensible importance values for both the gating variable c and the conditioned variables x and y across target levels γ' . The results for varying γ are presented and discussed in Appendix C.1, where we also observe condPED-ANOVA consistently shows reasonable behavior.

5.3 Regime-Dependent Domains

5.3.1 Problem Setting. We consider a synthetic optimization problem in which the domains of hyperparameters change depending on a gating variable.

The objective is to minimize:

$$f(c, x, y) = x + y, \quad (9)$$

with the following regime-dependent domains:

$$c \in [0, 1], \begin{cases} x \in [-7, -2], y \in [-5, -2], & \text{if } c < 0.5, \\ x \in [2, 7], y \in [2, 5], & \text{if } c \geq 0.5. \end{cases} \quad (10)$$

Here, both x and y are always present, but their feasible ranges switch according to c .

5.3.2 Results and Discussion. The results are shown in Figure 1c. Similar to the disjoint-domain setting (Equation (7)) in the conditional activation experiment (Section 5.2), the gating variable c determines whether a sample achieves top-half performance, which is reflected by the high importance of c around $\gamma' \approx 0.5$. On the other hand, unlike the conditional activation case, both x and y are always active and contribute to the objective, so their importance grows toward more extreme targets (smaller or larger γ'). Moreover, x is consistently more important than y , reflecting its ability to attain more extreme values (around ± 7).

5.4 Comparison with Existing Methods

5.4.1 Baselines. We compare condPED-ANOVA with existing HPI estimators. Since none of the standard HPI methods are designed to handle conditional hyperparameters in a principled manner, we

evaluate them under common naive extensions that enable their application to conditional search spaces.

We consider the following four baselines:

- **PED-ANOVA** [42], the original PED-ANOVA method;
- **f-ANOVA** [16], which estimates HPI via functional ANOVA decomposition on a random forest surrogate;
- **MDI** [24], the mean decrease impurity feature importance computed from a random forest surrogate; and
- **SHAP** [25], which assigns importance based on Shapley values [33] computed from a surrogate model, measuring each variable’s average marginal contribution.

For hyperparameters whose presence changes depending on other variables, we use the following two naive extensions:

- **Filtering:** From the evaluation set $\{(x_n, f(x_n))\}_{n=1}^N$, we keep only samples in which the target hyperparameter is present, and compute HPI on the filtered subset.
- **Imputation:** For samples in which the target hyperparameter is inactive, we impute its value by a default value (the midpoint of its domain) and compute HPI on the resulting completed dataset.

For hyperparameters whose domain switches across regimes, we use the following naive extension:

- **Expansion:** We treat the hyperparameter as if it were sampled from a single expanded domain that covers all regime-specific ranges, and compute HPI on this unified representation.

The pseudocodes of these naive extensions are provided in Appendix D.2. Consequently, for conditional activation, we obtain $4 \times 2 = 8$ baseline variants (four HPI methods combined with two naive handling schemes), whereas for regime-dependent domains, we obtain $4 \times 1 = 4$ variants (four HPI methods combined with the expansion scheme), which we compare against condPED-ANOVA. See Appendix D.2 for further details on the experimental setup.

5.4.2 Results and Discussion. We first analyze the results on the conditional activation objective (Equation (6)) under the disjoint-domain setting (Equation (7)). As shown in Figure 2, applying simple filtering to the original PED-ANOVA leads to almost identical HPI values for x and y . This behavior is clearly undesirable: in order to achieve better performance (i.e., smaller γ'), the hyperparameter y is inactive, and tuning y cannot affect the objective value at all. This failure arises because filtering discards information about

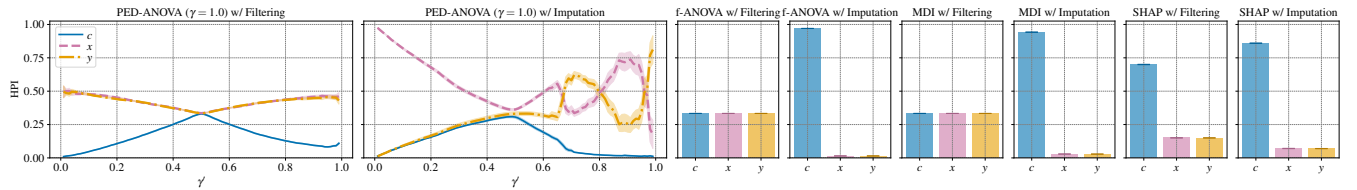


Figure 2: Baseline HPIs computed with naive extensions for existing methods for the synthetic objective with conditional activation (Equation (6)) under the disjoint domain setting (Equation (7)). “Filtering” computes HPI on the subset of samples where the target hyperparameter is active, whereas “Imputation” assigns a default value (the domain midpoint) to inactive samples before computing HPI. The lines and bars denote the mean, and the shaded regions and error bars denote the standard error, both computed over ten independent runs with different random seeds.

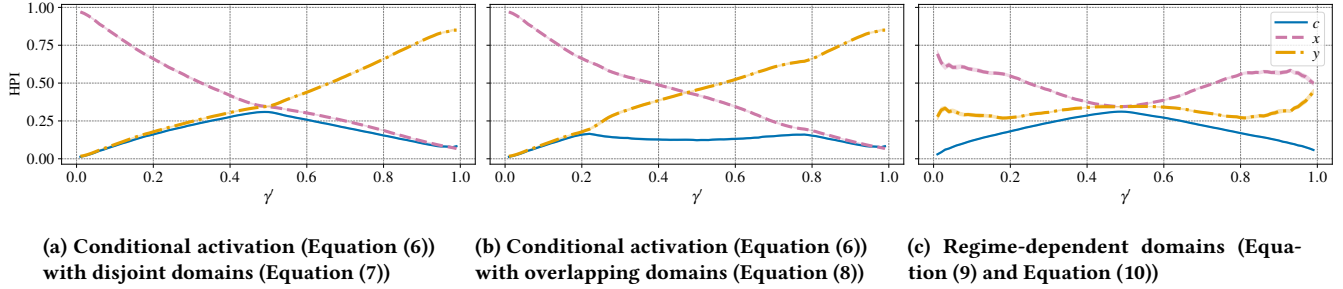


Figure 3: Ablation study results obtained using standard local HPI instead of conditional local HPI we defined in Section 4.2. The lines denote the mean, and the shaded regions denote the standard error, both computed over ten independent runs with different random seeds.

how the presence or absence of the variable relates to the overall performance landscape.

When imputation is applied instead, PED-ANOVA assigns a higher HPI to x in the small- γ' regime, which is qualitatively reasonable. However, the method still assigns a non-negligible importance to y and it becomes comparable to that of c , even though y should be inactive in this region. Moreover, for $\gamma' > 0.5$, the HPI of x and y exhibit substantial instability. These behaviors are caused by forcibly imputing an artificial value (the midpoint of the domain) for inactive configurations, which distorts the empirical sample distribution and introduces spurious dependencies.

Furthermore, in both filtering and imputation extensions of PED-ANOVA, the hyperparameter c , which solely determines whether the objective value belongs to the top-performing half, is not properly identified as important. Around $\gamma' \approx 0.5$, all hyperparameters are assigned nearly identical HPI values, indicating a complete failure to capture the dominant role of c in controlling performance.

Similar issues are observed for the other baseline estimators. For f-ANOVA and MDI with filtering, all hyperparameters receive identical importance values, while all the remaining variants still assign identical HPI values to x and y .

These results demonstrate that naive extensions are insufficient for adapting existing HPI estimators to conditional search spaces and fail to produce meaningful or interpretable importance estimates. In contrast, condPED-ANOVA consistently yields meaningful importance values that reflect the underlying conditional structure (as shown in Section 5.2). Further discussion on the other objectives and domain settings is deferred to Appendix C.2, where we observe the baselines fail to yield meaningful HPI in conditional settings.

5.5 Ablation Study: Effect of Within-Regime Variance and Regime Weighting

In this section, we conduct ablation studies to examine the impact of key design choices in condPED-ANOVA, focusing on within-regime variance and regime-level weighting.

5.5.1 Effect of Within-Regime Variance for HPI. In Section 4.2, we defined the conditional local HPI using the within-regime local marginal variance $v_{y,\text{within}}^{(d)}$. We therefore compare the resulting

HPI estimates with those obtained using the standard local marginal variance $v_Y^{(d)}$. The closed-form expression for the standard local marginal variance, computed using the indicator function $b_{\gamma'} := 1\{\gamma' \in X_{\gamma'}\}$, is given as follows, where we can also derive a decomposition of the Pearson divergence into within-regime and inter-regime components (cf. Lemma E.2 in Appendix E.3):

$$v_Y^{(d)} = \left(\frac{\gamma'}{\gamma} \right)^2 \underbrace{\left(\sum_{i=1}^{K^{(d)}} \frac{(\alpha_i^{(d)})^2}{\beta_i^{(d)}} D_{\text{PE}}(p_{\gamma',i}^{(d)} \parallel p_{\gamma,i}^{(d)}) \right)}_{\text{within-regime divergence}} + \underbrace{D_{\text{PE}}(\boldsymbol{\alpha}^{(d)} \parallel \boldsymbol{\beta}^{(d)})}_{\text{inter-regime divergence}}, \quad (11)$$

where $\boldsymbol{\alpha}^{(d)} := (\alpha_1^{(d)}, \dots, \alpha_{K^{(d)}}^{(d)})$ and $\boldsymbol{\beta}^{(d)} := (\beta_1^{(d)}, \dots, \beta_{K^{(d)}}^{(d)})$.

The results obtained using the standard local marginal variance are shown in Figure 3. In both the conditional-activation setting with disjoint domains (Figure 3a) and the regime-dependent domain setting (Figure 3c), the HPI of the gating variable c is underestimated around $\gamma' \approx 0.5$ and becomes lower than those of x and y . This behavior is undesirable, since selecting the appropriate branch is crucial for achieving median-level performance. Moreover, in the conditional-activation setting (Figures 3a and 3b), the importance of x or y does not vanish even in the regions where the variable is inactive and is assigned non-zero HPIs, which are even larger than that of c (e.g., y for $\gamma' < 0.5$ and x for $\gamma' > 0.5$ in Figure 3a, and y for $\gamma' \lesssim 0.2$ and x for $\gamma' \gtrsim 0.8$ in Figure 3b). This happens because the inter-regime variance is primarily induced by the gating variable c . When HPI is computed using the standard local marginal variance that includes this inter-regime component, the effect of c leaks into the HPI estimates for x and y . As a result, c is suppressed by x and y in the region where c should be most important, and x and y receive spurious non-zero importance even in the regions where they should be inactive and have zero effect. This phenomenon can also be established mathematically. Theorem E.1 shows that, under the standard local marginal variance, the variance of a conditioned hyperparameter includes the gating variance as an additive term, which explains the observed leakage and the resulting misattribution of importance. Therefore, in conditional settings, it is essential

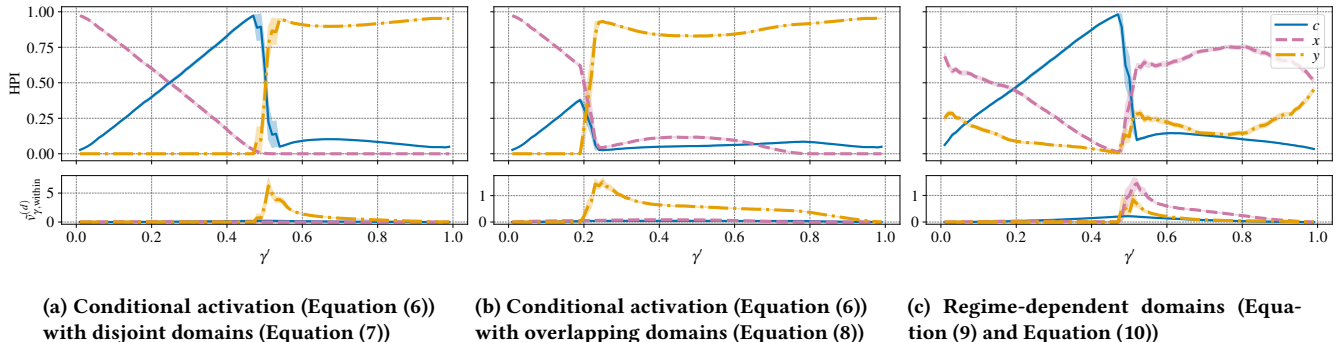


Figure 4: Ablation study results obtained by using the naive aggregation scheme (Equation (12)) instead of our closed-form expression (Theorem 4.2). The bottom row shows the HPIS before normalization, i.e., $\tilde{v}_{y,within}^{(d)}$. The lines denote the mean, and the shaded regions denote the standard error, both computed over ten independent runs with different random seeds.

to compute HPI using the within-regime local marginal variance $v_{y,within}^{(d)}$, rather than the standard local marginal variance $v_y^{(d)}$.

5.5.2 Effect of Regime-Level Weighting for HPI. In Section 4.3, we derived a closed-form computation method for $v_{y,within}^{(d)}$ based on a mathematical derivation (Theorem 4.2). However, one might wonder whether such a derivation is necessary in practice, and instead consider a naive alternative that simply sums the within-regime Pearson divergences, i.e., using:

$$\tilde{v}_{y,within}^{(d)} = \left(\frac{\gamma'}{\gamma}\right)^2 \sum_{i=1}^{K^{(d)}} D_{PE}\left(p_{\gamma',i}^{(d)} \parallel p_{\gamma,i}^{(d)}\right) \quad (12)$$

in place of Equation (5). In this section, we empirically compare condPED-ANOVA against this naive aggregation scheme.

The results obtained using this naive aggregation scheme are shown in Figure 4. In this case, the resulting HPI curves become noticeably less stable and exhibit near-discontinuous changes around regime-switching boundaries. In particular, for the conditional-activation objective under the overlapping-domain setting (Equations (6) and (8)), the importance of y spikes immediately when y becomes active, excessively dominating the HPI and suppressing the importances of x and c , which should still contribute to the objective. Moreover, although the objective is symmetric between the top region ($\gamma' < 0.5$) and the bottom region ($\gamma' > 0.5$) across all settings, the naive scheme breaks this symmetry too severely, yielding clearly distorted importance patterns.

This instability is largely driven by abrupt scale changes at regime boundaries. As shown in the bottom row of Figure 4, $\tilde{v}_{y,within}^{(d)}$ for x and y exhibit implausible jumps at these boundaries, in sharp contrast to the regime-probability-weighted condPED-ANOVA (cf. Figure 9 in Appendix C.4). This failure occurs because removing the regime-probability ratios destroys the frequency-aware weighting across regimes, leading to an inappropriate aggregation that cannot properly account for regime prevalence.

6 Conclusion

We studied HPI estimation in conditional search spaces, where hyperparameters may appear, disappear, or change domain depending

on other choices. We identified a fundamental pitfall of standard local HPI: conditioning effects can leak into conditioned hyperparameters, leading to misleading importances. To address this, we defined conditional local HPI and proposed condPED-ANOVA, a closed-form, PED-ANOVA-style estimator that correctly handles conditional search spaces while retaining efficiency. Empirically, condPED-ANOVA yielded meaningful importances consistent with the underlying conditional structure, whereas naive extensions of existing estimators, including PED-ANOVA, often violated conditional semantics and produced distorted importances. We believe condPED-ANOVA serves as a practical and principled foundation for reliable HPI analysis in HPO workflows with conditional search spaces.

References

- [1] Takuya Akiba, Shotaro Sano, Toshihiko Yanase, Takeru Ohta, and Masanori Koyama. 2019. Optuna: A Next-Generation Hyperparameter Optimization Framework. In *The 25th ACM SIGKDD International Conference on Knowledge Discovery & Data Mining*. 2623–2631.
- [2] James Bergstra, Rémi Bardenet, Yoshua Bengio, and Balázs Kégl. 2011. Algorithms for hyper-parameter optimization. *Advances in neural information processing systems* 24 (2011).
- [3] James Bergstra and Yoshua Bengio. 2012. Random Search for Hyper-Parameter Optimization. *Journal of Machine Learning Research* 13, 10 (2012), 281–305.
- [4] James Bergstra, Daniel Yamins, and David Cox. 2013. Making a science of model search: Hyperparameter optimization in hundreds of dimensions for vision architectures. In *International conference on machine learning*. PMLR, 115–123.
- [5] André Biedenkapp, Marius Lindauer, Katharina Eggensperger, Frank Hutter, Chris Fawcett, and Holger Hoos. 2017. Efficient Parameter Importance Analysis via Ablation with Surrogates. In *Proceedings of the AAAI Conference on Artificial Intelligence*, Vol. 31. doi:10.1609/aaai.v31i1.10657
- [6] André Biedenkapp, Joshua Marben, Marius Lindauer, and Frank Hutter. 2019. CAVE: Configuration Assessment, Visualization and Evaluation. In *Learning and Intelligent Optimization: 12th International Conference, LION 12, Kalamata, Greece, June 10–15, 2018, Revised Selected Papers*. Springer-Verlag, 115–130. doi:10.1007/978-3-030-05348-2_10
- [7] Leo Breiman. 2001. Random Forests. *Machine Learning* 45, 1 (2001), 5–32. doi:10.1023/A:1010933404324
- [8] Brent Komer, James Bergstra, and Chris Eliasmith. 2014. Hyperopt-Sklearn: Automatic Hyperparameter Configuration for Scikit-Learn. In *Proceedings of the 13th Python in Science Conference*. 32–37. doi:10.25080/Majora-14bd3278-006
- [9] Stefan Falkner, Aaron Klein, and Frank Hutter. 2018. BOHB: Robust and Efficient Hyperparameter Optimization at Scale. In *Proceedings of the 35th International Conference on Machine Learning (Proceedings of Machine Learning Research, Vol. 80)*. PMLR, 1437–1446.
- [10] Chris Fawcett and Holger H. Hoos. 2016. Analysing differences between algorithm configurations through ablation. *Journal of Heuristics* 22, 4 (2016), 431–458. doi:10.1007/s10732-014-9275-9

[11] Matthias Feurer, Katharina Eggensperger, Stefan Falkner, Marius Lindauer, and Frank Hutter. 2022. Auto-sklearn 2.0: hands-free AutoML via meta-learning. *Journal of Machine Learning Research* 23, 1, Article 261 (2022), 61 pages.

[12] Matthias Feurer, Aaron Klein, Katharina Eggensperger, Jost Springenberg, Manuel Blum, and Frank Hutter. 2015. Efficient and Robust Automated Machine Learning. In *Advances in Neural Information Processing Systems*, Vol. 28. Curran Associates, Inc.

[13] Peter Henderson, Riahat Islam, Philip Bachman, Joelle Pineau, Doina Precup, and David Meger. 2018. Deep reinforcement learning that matters. In *Proceedings of the AAAI Conference on Artificial Intelligence*. AAAI Press, Article 392, 8 pages.

[14] Giles Hooker. 2007. Generalized functional anova diagnostics for high-dimensional functions of dependent variables. *Journal of computational and graphical statistics* 16, 3 (2007), 709–732.

[15] Jianhua Z Huang. 1998. Projection estimation in multiple regression with application to functional ANOVA models. *The annals of statistics* 26, 1 (1998), 242–272.

[16] Frank Hutter, Holger Hoos, and Kevin Leyton-Brown. 2014. An efficient approach for assessing hyperparameter importance. In *International conference on machine learning*. PMLR, 754–762.

[17] Frank Hutter, Holger H. Hoos, and Kevin Leyton-Brown. 2013. Identifying Key Algorithm Parameters and Instance Features Using Forward Selection. In *Learning and Intelligent Optimization*. Springer Berlin Heidelberg, 364–381.

[18] Frank Hutter, Lars Kotthoff, and Joaquin Vanschoren. 2019. *Automated Machine Learning: Methods, Systems, Challenges* (1st ed.). Springer Publishing Company, Incorporated.

[19] Rodolphe Jenatton, Cedric Archambeau, Javier González, and Matthias Seeger. 2017. Bayesian Optimization with Tree-structured Dependencies. In *Proceedings of the 34th International Conference on Machine Learning (Proceedings of Machine Learning Research*, Vol. 70). PMLR, 1655–1664.

[20] Lars Kotthoff, Chris Thornton, Holger H. Hoos, Frank Hutter, and Kevin Leyton-Brown. 2017. Auto-WEKA 2.0: Automatic model selection and hyperparameter optimization in WEKA. *Journal of Machine Learning Research* 18, 25 (2017), 1–5.

[21] Lisha Li, Kevin Jamieson, Giulia DeSalvo, Afshin Rostamizadeh, and Ameet Talwalkar. 2018. Hyperband: A Novel Bandit-Based Approach to Hyperparameter Optimization. *Journal of Machine Learning Research* 18, 185 (2018), 1–52.

[22] Marius Lindauer, Katharina Eggensperger, Matthias Feurer, AndrÃ© Biedenkapp, Difan Deng, Carolin Benjamins, Tim Ruhkopf, RenÃ© Sass, and Frank Hutter. 2022. SMAC3: A Versatile Bayesian Optimization Package for Hyperparameter Optimization. *Journal of Machine Learning Research* 23, 54 (2022), 1–9.

[23] Marius Lindauer, Katharina Eggensperger, Matthias Feurer, AndrÃ© Biedenkapp, Joshua Marben, Philipp MÃ¼ller, and Frank Hutter. 2019. BOAH: A Tool Suite for Multi-Fidelity Bayesian Optimization & Analysis of Hyperparameters. *arXiv preprint arXiv:1908.06756* (2019).

[24] Gilles Louppe, Louis Wehenkel, Antonio Sutera, and Pierre Geurts. 2013. Understanding variable importances in forests of randomized trees. In *Advances in Neural Information Processing Systems*, Vol. 26.

[25] Scott M Lundberg and Su-In Lee. 2017. A Unified Approach to Interpreting Model Predictions. In *Advances in Neural Information Processing Systems*, Vol. 30.

[26] Xingchen Ma and Matthew Blaschko. 2020. Additive Tree-Structured Covariance Function for Conditional Parameter Spaces in Bayesian Optimization. In *Proceedings of the Twenty Third International Conference on Artificial Intelligence and Statistics (Proceedings of Machine Learning Research*, Vol. 108). PMLR, 1015–1025.

[27] Gábor Melis, Chris Dyer, and Phil Blunsom. 2018. On the State of the Art of Evaluation in Neural Language Models. In *International Conference on Learning Representations*.

[28] Julia Moosbauer, Julia Herbinger, Giuseppe Casalicchio, Marius Lindauer, and Bernd Bischl. 2021. Explaining Hyperparameter Optimization via Partial Dependence Plots. In *Advances in Neural Information Processing Systems*, Vol. 34, 2280–2291.

[29] Philipp Probst, Anne-Laure Boulesteix, and Bernd Bischl. 2019. Tunability: Importance of Hyperparameters of Machine Learning Algorithms. *Journal of Machine Learning Research* 20, 53 (2019), 1–32.

[30] Julian Rodemann, Federico Croppi, Philipp Arens, Yusuf Sale, Julia Herbinger, Bernd Bischl, Eyke Hüllermeier, Thomas Augustin, Conor J. Walsh, and Giuseppe Casalicchio. 2026. Explaining Bayesian Optimization by Shapley Values Facilitates Human-AI Collaboration for Exosuit Personalization. In *Machine Learning and Knowledge Discovery in Databases. Research Track and Applied Data Science Track*. Springer Berlin Heidelberg, 525–542.

[31] David W. Scott. 1992. *Multivariate Density Estimation: Theory, Practice, and Visualization*. John Wiley & Sons. doi:10.1002/9780470316849

[32] Sarah Segel, Helena Graf, Alexander Tornede, Bernd Bischl, and Marius Lindauer. 2023. Symbolic Explanations for Hyperparameter Optimization. In *Proceedings of the Second International Conference on Automated Machine Learning (Proceedings of Machine Learning Research*, Vol. 224). PMLR, 2/1–22.

[33] L. S. Shapley. 1953. *A Value for n-Person Games*. Princeton University Press, Princeton, 307–318. doi:doi:10.1515/9781400881970-018

[34] Jasper Snoek, Hugo Larochelle, and Ryan P Adams. 2012. Practical Bayesian Optimization of Machine Learning Algorithms. In *Advances in Neural Information Processing Systems*, F. Pereira, C.J. Burges, L. Bottou, and K.Q. Weinberger (Eds.), Vol. 25.

[35] Illya M Sobol. 1993. Sensitivity estimates for nonlinear mathematical models, Mathematical Modeling and Computational Experiment. *Mathematical Modeling and Computational Experiment* (1993), 407–414.

[36] Illya M Sobol. 2001. Global sensitivity indices for nonlinear mathematical models and their Monte Carlo estimates. *Mathematics and computers in simulation* 55, 1-3 (2001), 271–280.

[37] Carolin Strobl, Anne-Laure Boulesteix, Achim Zeileis, and Torsten Hothorn. 2007. Bias in random forest variable importance measures: Illustrations, sources and a solution. *BMC Bioinformatics* 8, 1 (2007), 25. doi:10.1186/1471-2105-8-25

[38] Kevin Swersky, David Duvenaud, Jasper Snoek, Frank Hutter, and Michael A. Osborne. 2014. Raiders of the Lost Architecture: Kernels for Bayesian Optimization in Conditional Parameter Spaces. *arXiv preprint arXiv:1409.4011* (2014).

[39] Daphne Theodorakopoulou, Frederic Stahl, and Marius Lindauer. 2024. Hyperparameter Importance Analysis for Multi-Objective AutoML. In *European Conference on Artificial Intelligence*. IOS Press. doi:10.3233/faia240602

[40] Chris Thornton, Frank Hutter, Holger H. Hoos, and Kevin Leyton-Brown. 2013. Auto-WEKA: combined selection and hyperparameter optimization of classification algorithms. In *Proceedings of the 19th ACM SIGKDD International Conference on Knowledge Discovery and Data Mining*, 847–855. doi:10.1145/2487575.2487629

[41] Jan N Van Rijn and Frank Hutter. 2018. Hyperparameter importance across datasets. In *Proceedings of the 24th ACM SIGKDD international conference on knowledge discovery & data mining*, 2367–2376.

[42] Shuhei Watanabe, Archit Bansal, and Frank Hutter. 2023. PED-ANOVA: Efficiently quantifying hyperparameter importance in arbitrary subspaces. In *Proceedings of the Thirty-Second International Joint Conference on Artificial Intelligence*, 4389–4396.

[43] Marcel Wever, Maximilian Muschalik, Fabian Fumagalli, and Marius Lindauer. 2026. HyperSHAP: Shapley Values and Interactions for Explaining Hyperparameter Optimization. In *Proceedings of the AAAI Conference on Artificial Intelligence*. To appear.

[44] Lucas Zimmer, Marius Lindauer, and Frank Hutter. 2021. Auto-Pytorch: Multi-Fidelity MetaLearning for Efficient and Robust AutoDL. *IEEE Transactions on Pattern Analysis and Machine Intelligence* 43, 9 (2021), 3079–3090. doi:10.1109/TPAMI.2021.3067763

A Additional Related Work

A.1 Contrastive Hyperparameter Importance

Beyond global variance-based rankings, several lines of work emphasize selection, contrastive explanations, or local sensitivity. Hutter et al. [17] study *forward selection* to identify a small subset of influential inputs (parameters and instance features) by incrementally adding dimensions that most improve surrogate predictive accuracy, followed by a drop-one analysis to rank selected inputs. In parallel, *ablation analysis* [10] explains performance differences between two high-quality configurations by constructing a path that sequentially ablates parameter changes and quantifies their contributions, yielding a contrastive, configuration-to-configuration notion of importance. Biedenkapp et al. [5] accelerate this paradigm via *ablation with surrogates*, replacing expensive evaluations with model-based predictions to achieve large speedups while maintaining explanatory utility. To further focus on neighborhood behavior, CAVE [6] introduces local parameter importance, which measures variance in predicted performance when varying one parameter around a specific configuration, and empirically argues that local and global importance can disagree and thus complement each other.

A.2 Importance Across Datasets and Tunability

Another line of work studies importance beyond a single dataset or run. Van Rijn and Hutter [41] aggregates evidence across many datasets (via OpenML metadata) to identify which hyperparameters tend to matter most for an algorithm in general, and to infer

priors over promising values; this reframes HPI as a meta-learning problem and supports more data-driven space design and warm-starting. Complementarily, [29] introduce tunability measures that quantify how much performance can improve by tuning, providing a practitioner-facing notion of “which hyperparameters are worth tuning” and offering data-based defaults and empirical assessments across datasets and algorithms.

A.3 Explainable HPO via Partial Dependence and Symbolic Models

In parallel, a growing body of work tackles explainability of HPO using tools from interpretable machine learning. Moosbauer et al. [28] study partial dependence plots (PDPs) for explaining BO-based HPO runs and show that naive PDPs can be biased due to the non-uniform, sequential sampling of BO. They propose uncertainty-aware PDPs based on the BO surrogate, together with a partitioning of the hyperparameter space into subregions where the surrogate is more reliable, to obtain more trustworthy visual summaries of marginal hyperparameter effects. Segel et al. [32] go one step further and introduce symbolic explanations for HPO: using symbolic regression on meta-data collected from BO runs, they learn compact analytic formulas that approximate the relationship between hyperparameters and performance, thereby providing globally interpretable, human-readable explanations that complement fANOVA-style variance decompositions and PDP-based visualizations.

A.4 Tree-Based Feature Importances

A widely used family of importance measures arises from tree ensembles such as random forests [7]. In particular, the mean decrease impurity (MDI) ranks variables by aggregating their impurity reductions over splits across the ensemble. MDI is popular due to its simplicity and low computational cost, and has been theoretically characterized for randomized trees as a variance decomposition under asymptotic conditions [24]. At the same time, impurity-based importances can exhibit biases (e.g., with respect to variable scale or cardinality), motivating careful interpretation and alternative corrections [37].

A.5 Game-Theoretic Explanations for HPI

Game-theoretic attribution methods provide another approach to importance. The Shapley value [33] offers an axiomatic way to assign each feature its average marginal contribution to a model output. In machine learning, SHAP [25] leverages Shapley values to produce feature attributions for individual predictions, and global importance scores can be obtained by aggregating these local attributions across data. These Shapley-based scores are increasingly used as surrogate-based importance baselines in interpretability.

Within HPO, Rodemann et al. [30] propose ShapleyBO, explaining Bayesian optimization proposals by attributing each parameter’s contribution to the acquisition function rather than to model predictions, and further decomposing contributions into exploration vs. exploitation terms for additive acquisition functions. More directly for HPI, HyperSHAP [43] uses Shapley values and Shapley interaction indices to provide additive decompositions of a performance measure over hyperparameters, aiming to support both local and global explanations, including interactions.

A.6 Multi-Objective HPI

For multi-objective HPO, Theodorakopoulos et al. [39] propose a framework that computes HPI across objective trade-offs by applying surrogate-based importance measures (notably f-ANOVA and ablation paths) to scalarized objectives, thereby producing importance profiles that vary with the weighting of competing objectives.

B Rigorous Details of condPED-ANOVA

We briefly presented an overview of condPED-ANOVA in Section 4. Here, we provide the rigorous details of the method.

For simplicity, we omit the boldface notation for vectors x . We assume that the objective function f is measurable.

B.1 Extended One-Dimensional Domain

Section 4.1 introduced a regime-based representation of conditional hyperparameters. Here, we provide a rigorous formulation of the corresponding hyperparameter search space. This formalization is necessary to define the empirical distributions $\mu_{\gamma'}^{(d)}$ and $\mu_{\gamma}^{(d)}$ (and corresponding PDFs $p_{\gamma'}$ and p_{γ}) over a conditional search space, which underlies the subsequent derivations.

We assume that the d -th hyperparameter can be in one of $K^{(d)} \in \mathbb{N}$ regimes. Formally, let $r^{(d)} : \mathcal{X} \rightarrow \{1, \dots, K^{(d)}\}$ be a measurable regime function that specifies the regime of the d -th hyperparameter for each configuration $x \in \mathcal{X}$. Each regime $i \in \{1, \dots, K^{(d)}\}$ is associated with its own domain $\mathcal{Z}_i^{(d)}$, which may differ across regimes.

To capture both regime information and regime-specific domain in a single one-dimensional object, we introduce an *extended domain* for the d -th hyperparameter as:

$$S^{(d)} := \bigsqcup_{i=1}^{K^{(d)}} (\{i\} \times \mathcal{Z}_i^{(d)}),$$

where \bigsqcup denotes a disjoint union, so that different regimes are treated as separate components even if their numeric domains may overlap. We equip $S^{(d)}$ with the σ -algebra induced by the disjoint union, so that each partition element $A_i^{(d)} := \{i\} \times \mathcal{Z}_i^{(d)} \subset S^{(d)}$ is measurable.

B.2 Rigorous Formulation of condPED-ANOVA

Let $\mu_{\gamma'}^{(d)}$ and $\mu_{\gamma}^{(d)}$ denote the empirical distributions of the extended d -th hyperparameter on $S^{(d)}$ induced by the top- γ' and top- γ subsets, respectively. These correspond to densities $p_{\gamma'}$ and p_{γ} introduced in Section 4 with respect to a suitable reference measure.

For each regime i , recall the measurable component $A_i^{(d)} \subset S^{(d)}$ and define the regime probabilities:

$$\alpha_i^{(d)} := \mu_{\gamma'}^{(d)}(A_i^{(d)}), \quad \text{and} \quad \beta_i^{(d)} := \mu_{\gamma}^{(d)}(A_i^{(d)}).$$

Whenever $\alpha_i^{(d)} > 0$ and $\beta_i^{(d)} > 0$, define the conditional (restricted) measures:

$$\mu_{\gamma',i}^{(d)} := \mu_{\gamma'}^{(d)}(\cdot | A_i^{(d)}), \quad \text{and} \quad \mu_{\gamma,i}^{(d)} := \mu_{\gamma}^{(d)}(\cdot | A_i^{(d)}).$$

If $\alpha_i^{(d)} = 0$, we do not need to define $\mu_{\gamma',i}^{(d)}$ since its contribution vanishes in Equation (14) through the factor $(\alpha_i^{(d)})^2$. Since $S^{(d)} =$

$\bigsqcup_{i=1}^{K^{(d)}} A_i^{(d)} = \bigsqcup_{i=1}^{K^{(d)}} (\{i\} \times \mathcal{Z}_i^{(d)})$ forms a disjoint partition, we obtain the following regime-wise decomposition of the marginals:

$$\mu_{Y'}^{(d)} = \sum_{i=1}^{K^{(d)}} \alpha_i^{(d)} \mu_{Y',i}^{(d)}, \quad \text{and} \quad \mu_Y^{(d)} = \sum_{i=1}^{K^{(d)}} \beta_i^{(d)} \mu_{Y,i}^{(d)}. \quad (13)$$

Note that we have the absolute continuity $\mu_{Y'}^{(d)} \ll \mu_Y^{(d)}$, since $\mathcal{X}_{Y'} \subset \mathcal{X}_Y$. The regime-wise $\mu_{Y',i}^{(d)} \ll \mu_{Y,i}^{(d)}$ also holds for all regimes with $\beta_i > 0$, since absolute continuity is preserved under restriction to measurable subsets.

With these definitions, we obtain the following closed-form expression for the within-regime local marginal variance:

THEOREM B.1 (CONDPED-ANOVA (RESTATE)). *Let $0 < \gamma' < \gamma \leq 1$. The within-regime local marginal variance for the d -th hyperparameter at level γ , computed using the indicator function $b_{Y'} := \mathbb{1}\{x \in \mathcal{X}_{Y'}\}$, is given by:*

$$v_{Y,\text{within}}^{(d)} = \left(\frac{\gamma'}{\gamma}\right)^2 \sum_{i: \beta_i^{(d)} > 0} \frac{(\alpha_i^{(d)})^2}{\beta_i^{(d)}} D_{\text{PE}}\left(\mu_{Y',i}^{(d)} \middle\| \mu_{Y,i}^{(d)}\right), \quad (14)$$

Here, the Pearson (χ^2) divergence is defined as:

$$D_{\text{PE}}(\nu \middle\| \mu) := \int \left(\frac{dv}{d\mu} - 1 \right)^2 d\mu,$$

for probability measures ν and μ with $\nu \ll \mu$. Note that the summation in Equation (14) is restricted to regimes with $\beta_i^{(d)} > 0$; regimes absent from the top- γ set contribute neither to the within-regime variance nor to the divergence. If $A_i^{(d)}$ corresponds to an inactive configuration (i.e., $\mathcal{Z}_i^{(d)} = \{\perp\}$), then $\mu_{Y,i}^{(d)}$ and $\mu_{Y',i}^{(d)}$ are both degenerate on $A_i^{(d)}$, implying $D_{\text{PE}}(\mu_{Y',i}^{(d)} \middle\| \mu_{Y,i}^{(d)}) = 0$. When $K^{(d)} = 1$, we have $\alpha_1 = \beta_1 = 1$ and Equation (14) reduces to the original PED-ANOVA expression.

In practice, the sample size within each regime $A_i^{(d)}$ must be large enough for KDE to be stable. When the domains $\mathcal{Z}_i^{(d)}$ vary continuously with other coordinates, it is often preferable to discretize them into fixed intervals so that sufficient samples can be pooled within each regime.

B.3 Proof of Theorem B.1

PROOF. Let S be a random element distributed according to the empirical distribution $\mu_Y^{(d)}$ on $S^{(d)}$ induced by the top- γ subset. Let $Y \in \{0, 1\}$ indicate whether the underlying sample comes from the tighter top set, i.e., $Y = 1$ corresponds to membership in the top- γ' subset. By definition, the conditional law of S given $Y = 1$ is $\mu_{Y'}^{(d)}$. Let $\kappa := \mathbb{P}(Y = 1)$. By construction, $\kappa = |\mathcal{D}_{Y'}| / |\mathcal{D}_Y|$; under the quantile definition used in the main text, this equals γ'/γ up to the floor effect, and we use $\kappa = \gamma'/\gamma$ for simplicity.

For any measurable set $B \subset S^{(d)}$, we have:

$$\begin{aligned} \mathbb{P}(S \in B, Y = 1) &= \mathbb{P}(Y = 1) \mathbb{P}(S \in B \mid Y = 1) \\ &= \kappa \mu_{Y'}^{(d)}(B), \end{aligned}$$

and

$$\mathbb{P}(S \in B) = \mu_Y^{(d)}(B).$$

Since $\mathcal{X}_{Y'} \subset \mathcal{X}_Y$, we have $\mu_{Y'}^{(d)} \ll \mu_Y^{(d)}$, and thus the Radon-Nikodým derivative $d\mu_{Y'}^{(d)} / d\mu_Y^{(d)}$ exists. Thus, by the definition of conditional probability, for $s \in S^{(d)}$, we have:

$$\mathbb{P}(Y = 1 \mid S = s) = \kappa \frac{\mu_{Y'}^{(d)}}{\mu_Y^{(d)}}(s). \quad (15)$$

Since $S^{(d)} = \bigsqcup_{i=1}^{K^{(d)}} A_i^{(d)} = \bigsqcup_{i=1}^{K^{(d)}} (\{i\} \times \mathcal{Z}_i^{(d)})$ forms a disjoint partition (Equation (13)), the following factorization holds for each i with $\beta_i^{(d)} > 0$, for $s \in A_i^{(d)}$:

$$\frac{d\mu_{Y'}^{(d)}}{d\mu_Y^{(d)}}(s) = \frac{d(\alpha_i^{(d)} \mu_{Y',i}^{(d)})}{d(\beta_i^{(d)} \mu_{Y,i}^{(d)})}(s) = \frac{\alpha_i^{(d)}}{\beta_i^{(d)}} \frac{d\mu_{Y',i}^{(d)}}{d\mu_{Y,i}^{(d)}}(s), \quad (16)$$

Using Equation (15) and Equation (16), for each i with $\beta_i^{(d)} > 0$, for $s \in A_i^{(d)}$, we obtain:

$$\mathbb{P}(Y = 1 \mid S = s) = \kappa \frac{\alpha_i^{(d)}}{\beta_i^{(d)}} \frac{d\mu_{Y',i}^{(d)}}{d\mu_{Y,i}^{(d)}}(s)$$

Recall that the within-regime local HPI is defined as the within-regime variance of the conditional probability of being in the tighter top set, i.e.,

$$v_{Y,\text{within}}^{(d)} := \mathbb{E}_I [\text{Var}(\mathbb{P}(Y = 1 \mid S) \mid I)].$$

Taking expectation over I and using $\mathbb{P}(I = i) = \beta_i$ yields:

$$\begin{aligned} v_{Y,\text{within}}^{(d)} &= \sum_{i: \beta_i^{(d)} > 0} \beta_i^{(d)} \text{Var}_{s \sim \mu_{Y,i}^{(d)}} \left(\kappa \frac{\alpha_i^{(d)}}{\beta_i^{(d)}} \frac{d\mu_{Y',i}^{(d)}}{d\mu_{Y,i}^{(d)}}(s) \right) \\ &= \kappa^2 \sum_{i: \beta_i^{(d)} > 0} \frac{(\alpha_i^{(d)})^2}{\beta_i^{(d)}} \text{Var}_{s \sim \mu_{Y,i}^{(d)}} \left(\frac{d\mu_{Y',i}^{(d)}}{d\mu_{Y,i}^{(d)}}(s) \right) \\ &= \kappa^2 \sum_{i: \beta_i^{(d)} > 0} \frac{(\alpha_i^{(d)})^2}{\beta_i^{(d)}} \int \left(\frac{d\mu_{Y',i}^{(d)}}{d\mu_{Y,i}^{(d)}}(s) - 1 \right)^2 d\mu_{Y,i}^{(d)}(s) \\ &= \kappa^2 \sum_{i: \beta_i^{(d)} > 0} \frac{(\alpha_i^{(d)})^2}{\beta_i^{(d)}} D_{\text{PE}}\left(\mu_{Y',i}^{(d)} \middle\| \mu_{Y,i}^{(d)}\right). \end{aligned}$$

Here, we used the following equation, which holds since $\mu_{Y',i}^{(d)}$ is a probability measure:

$$\mathbb{E}_{s \sim \mu_{Y,i}^{(d)}} \left[\frac{d\mu_{Y',i}^{(d)}}{d\mu_{Y,i}^{(d)}}(s) \right] = \int \frac{d\mu_{Y',i}^{(d)}}{d\mu_{Y,i}^{(d)}} d\mu_{Y,i}^{(d)} = \mu_{Y',i}^{(d)}(S^{(d)}) = 1.$$

This completes the proof. \square

C Additional Results and Discussion on Numerical Experiments

C.1 condPED-ANOVA Results on Synthetic Objectives with Different γ Values

The results of condPED-ANOVA for the objective with conditional activation (Equation (6)) and the objective with regime-dependent domains (Equation (9)), with γ set to 0.75 and 0.5, are shown in Figure 5.

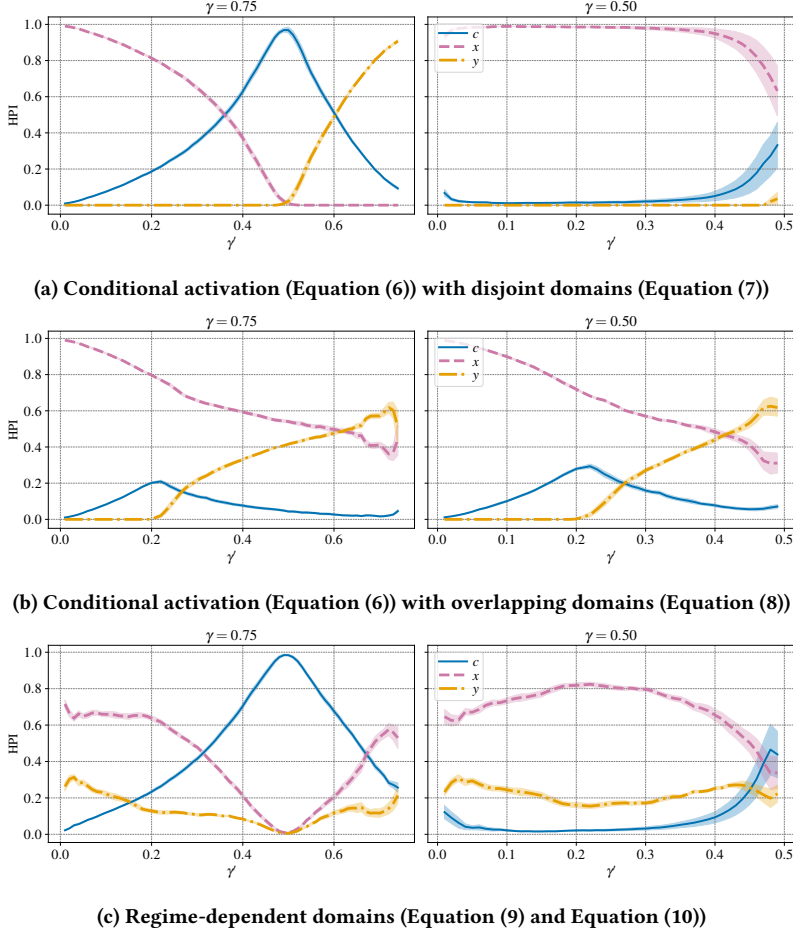


Figure 5: condPED-ANOVA HPI computed for the synthetic objectives. For the objective with conditional activation (Equation (6)), the gating hyperparameter c determines which branch is active: x is present only when $c < 0.5$, whereas y is present only when $c \geq 0.5$. For the objective with regime-dependent domains (Equation (9)), the gating hyperparameter c determines the domain of the hyperparameters x and y . The lines denote the mean, and the shaded regions denote the standard error, both computed over ten independent runs with different random seeds.

The results share some similarities with the higher- γ' range in Figure 1, which reflects the fact that varying γ changes the region over which HPI is computed. However, the behavior is not a simple zoom-in because the definition of the top- γ region itself changes. In particular, with $\gamma = 0.5$ in the disjoint-domain setting (Figure 5b, right panel), once we restrict attention to the better half of the evaluations (i.e., the region where $c < 0.5$ is already selected), adjusting c no longer changes the objective value. Accordingly, the importance of c becomes small in this regime, similar to the importance of y .

C.2 Comparison with Existing Methods

The results for the baseline methods described in Section 5.4 for the conditional-activation objective with the overlapping-domain setting (Equations (6) and (8)) and the regime-dependent domain setting (Equations (9) and (10)) are shown in Figures 6 and 7, respectively.

First, for the conditional-activation objective, we observe the same trend as in the disjoint-domain setting (Equations (6) and (7)). PED-ANOVA with filtering fails to distinguish between x and y , while PED-ANOVA with imputation assigns y an importance comparable to c in the small- γ' regime, where y should be inactive and thus cannot improve performance. Similarly, f-ANOVA with filtering and MDI with filtering again yield nearly identical HPI values for all hyperparameters, and the remaining baselines also tend to assign almost the same importance to x and y .

Next, for the regime-dependent domain setting, PED-ANOVA with expansion also behaves undesirably: although c determines whether a configuration falls into the top half, the importance of c around $\gamma' \approx 0.5$ becomes smaller than that of x and y . This failure is caused by expansion, which collapses the regime-specific ranges of x and y into a single unified domain and thereby obscures the effect of range switching, preventing accurate estimation of x and y in the regimes where their domains change. Moreover, for f-ANOVA,

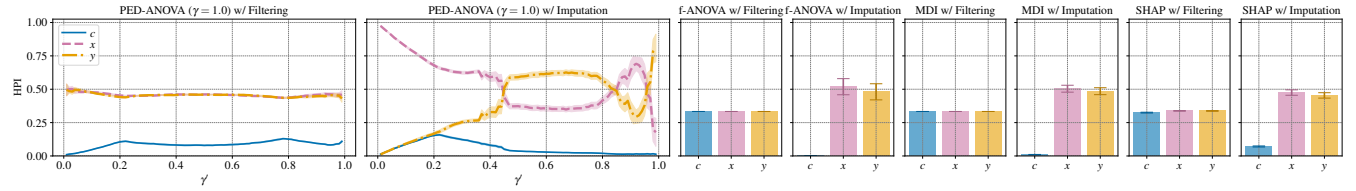


Figure 6: Baseline HPIs computed with naive extensions of existing methods for the synthetic objective with conditional activation (Equation (6)) under the overlapping domain setting (Equation (8)). The lines and bars denote the mean, and the shaded regions and error bars denote the standard error, both computed over ten independent runs with different random seeds.

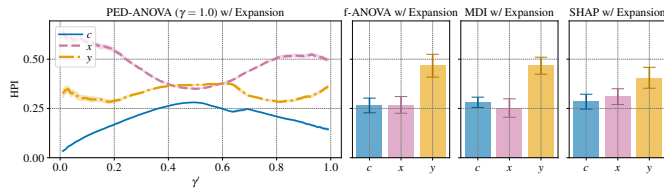


Figure 7: Baseline HPIs computed with naive extensions of existing methods for the synthetic objective with regime-dependent domains (Equation (9) and Equation (10)). The lines and bars denote the mean, and the shaded regions and error bars denote the standard error, both computed over ten independent runs with different random seeds.

MDI, and SHAP with expansion, y is assigned larger importance than x , even though x should contribute more to the objective. This is because forcibly expanding the domain distorts the relationship between the variables and the objective across regimes, leading to misleading HPI estimates.

These results indicate that the naive extensions do not provide meaningful HPI estimates that capture the difference between the contributions of x and y in this conditional setting, not only for the conditional-activation objective under the disjoint-domain setting (as shown in Section 5.4.2), but also under the overlapping-domain setting and in the regime-dependent domain setting.

C.3 Runtime Comparison

We compare the runtime of condPED-ANOVA against baseline HPI methods equipped with naive extensions on the synthetic objective with regime-dependent domains (Equation (9) and Equation (10)). For each sample size from 2^9 to 2^{17} , we measure the wall-clock time required to compute HPI, and report the results in Figure 8. f-ANOVA is reported only up to 2^{11} , since it could not be executed at larger sample sizes due to excessive memory consumption. Due to its substantial memory consumption, f-ANOVA could not be executed for larger sample sizes and is reported only up to 2^{11} . Similarly, SHAP is reported only up to 2^{15} because it was prohibitively slow at larger sample sizes.

In these results, condPED-ANOVA runs faster than all baseline methods across the evaluated ranges, indicating that the overhead introduced by our approach is small. Here, the fact that condPED-ANOVA is faster than PED-ANOVA indicates that the overhead of

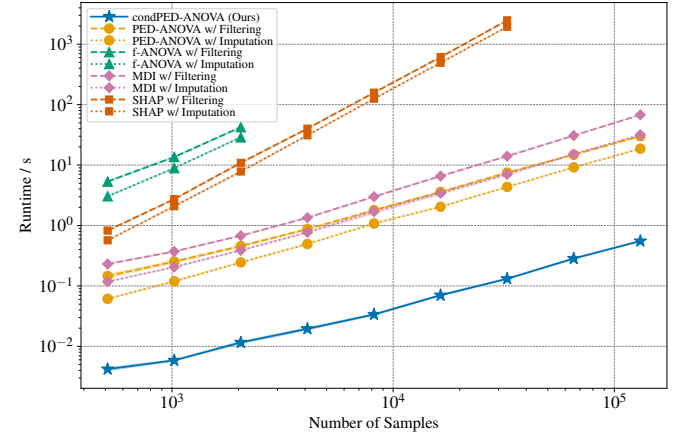


Figure 8: Runtime comparison against baseline HPI methods with naive extensions for the synthetic objective (Equation (9) and Equation (10)). The lines denote the mean, and the shaded regions denote the standard error, both computed over ten independent runs with different random seeds.

filtering or imputation is larger than the additional computation introduced by condPED-ANOVA.

C.4 Ablation Study on the Effect of Regime-Level Weighting

The ablation study results obtained by using a naive aggregation scheme (Equation (12)) instead of the closed-form expression derived in Theorem 4.2 are shown in Figure 4. For reference, we also show the HPI values before normalization, i.e., $\tilde{v}_{y,\text{within}}^{(d)}$, in Figure 9.

D Detailed Experimental Setup

D.1 Details for Common Experimental Setup

For estimating the PDFs $p_{Y',i}^{(d)}$ and $p_{Y,i}^{(d)}$, we use KDE with Optuna's default settings, which employ Scott's rule for bandwidth selection [31]. All experiments are run on a single machine with an Intel® Core™ Ultra 7 155H CPU (22 logical CPUs) and 16 GB RAM, running Arch Linux. We use Python version 3.13.11 and Optuna v4.7.0.

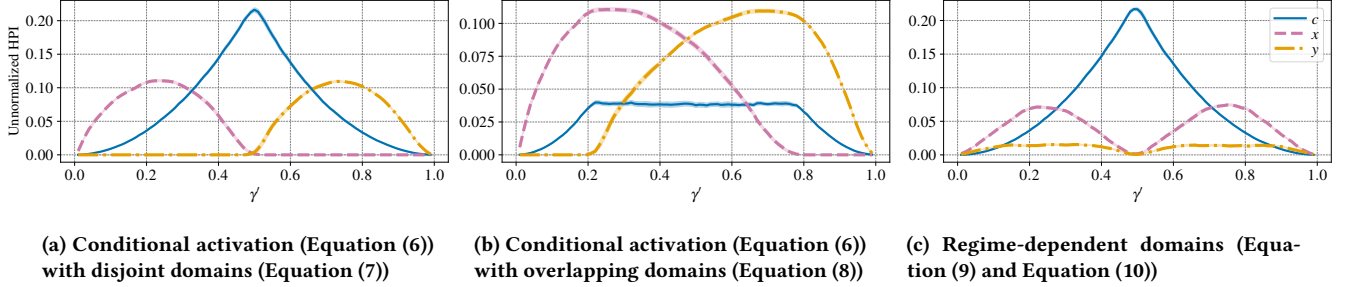


Figure 9: condPED-ANOVA ($\gamma = 1.0$) HPI values before normalization, i.e., $v_{\gamma, \text{within}}^{(d)}$, computed for the synthetic objectives. The lines denote the mean, and the shaded regions denote the standard error, both computed over ten independent runs with different random seeds.

D.2 Implementation Details for Baselines

For all four baseline methods, we use the implementations provided in Optuna [1] and follow Optuna’s default hyperparameter settings. The pseudocode for naive extension for these baselines is provided in Algorithms 2 to 4

Algorithm 2 Naive Extension: Filtering (Conditional Presence)

Input: Evaluation set $\mathcal{D} = \{(\mathbf{x}_n, f(\mathbf{x}_n))\}_{n=1}^N$, baseline evaluator $\text{BASELINEHPI}(\cdot)$

Output: Naive HPI for the hyperparameters \mathbf{x} via filtering

- 1: **for** $d = 1, \dots, D$ **do**
- 2: $\mathcal{D}_{\text{act}}^{(d)} \leftarrow \{(\mathbf{x}_n, f(\mathbf{x}_n)) \in \mathcal{D} \mid x_n^{(d)} \text{ is present}\}$ ▷ filtering
- 3: **if** $|\mathcal{D}_{\text{act}}^{(d)}| = 0$ **then**
- 4: $\text{HPI}^{(d)} \leftarrow 0$ ▷ no active trials; define HPI as zero
- 5: **else**
- 6: $\text{HPI} \leftarrow d\text{-th value of } \text{BASELINEHPI}(\mathcal{D}_{\text{act}}^{(d)})$
- 7: **end if**
- 8: **end for**
- 9: **return** $\{\text{HPI}^{(d)}\}_{d=1}^D$

Algorithm 3 Naive Extension: Imputation (Conditional Presence)

Input: Evaluation set $\mathcal{D} = \{(\mathbf{x}_n, f(\mathbf{x}_n))\}_{n=1}^N$, hyperparameter domains $\mathcal{X}^{(1)} \times \dots \times \mathcal{X}^{(D)} = [\ell^{(1)}, u^{(1)}] \times \dots \times [\ell^{(D)}, u^{(D)}]$, baseline evaluator $\text{BASELINEHPI}(\cdot)$

Output: Naive HPI for the hyperparameters via imputation

- 1: Initialize $\tilde{\mathcal{D}} \leftarrow \emptyset$
- 2: **for** $n = 1, \dots, N$ **do**
- 3: $\tilde{\mathbf{x}}_n \leftarrow \mathbf{x}_n$
- 4: **for** $d = 1, \dots, D$ **do**
- 5: **if** $x_n^{(d)}$ is inactive in \mathbf{x}_n **then**
- 6: ▷ imputation with the midpoint of the domain
- 7: Set $\tilde{x}_n^{(d)} \leftarrow (\ell^{(d)} + u^{(d)})/2$
- 8: **end if**
- 9: **end for**
- 10: $\tilde{\mathcal{D}} \leftarrow \tilde{\mathcal{D}} \cup \{(\tilde{\mathbf{x}}_n, f(\mathbf{x}_n))\}$
- 11: **end for**
- 12: **return** $\text{BASELINEHPI}(\tilde{\mathcal{D}})$

Algorithm 4 Naive Extension: Expansion (Regime-Specific Ranges)

Input: Evaluation set $\mathcal{D} = \{(\mathbf{x}_n, f(\mathbf{x}_n))\}_{n=1}^N$, regime-specific domains for each d -th hyperparameter $\{\mathcal{X}_i^{(d)} = [\ell_i^{(d)}, u_i^{(d)}]\}_{i=1}^{K^{(d)}}$, baseline evaluator $\text{BASELINEHPI}(\cdot)$

Output: Naive HPI for the hyperparameters via domain expansion

- 1: **for** $d = 1, \dots, D$ **do**
- 2: $\ell_{\min}^{(d)} \leftarrow \min_{i \in \{1, \dots, K^{(d)}\}} \ell_i^{(d)}$
- 3: $u_{\max}^{(d)} \leftarrow \max_{i \in \{1, \dots, K^{(d)}\}} u_i^{(d)}$
- 4: $\tilde{\mathcal{X}}^{(d)} = [\ell_{\min}^{(d)}, u_{\max}^{(d)}]$ ▷ expanded domain
- 5: **end for**
- 6: Initialize $\tilde{\mathcal{D}} \leftarrow \emptyset$
- 7: **for** $n = 1, \dots, N$ **do**
- 8: $\tilde{\mathbf{x}}_n \in \tilde{\mathcal{X}}^{(d)} \leftarrow \mathbf{x}_n$ ▷ treat each $x_n^{(d)}$ as a sample from $\tilde{\mathcal{X}}^{(d)}$
- 9: $\tilde{\mathcal{D}} \leftarrow \tilde{\mathcal{D}} \cup \{(\tilde{\mathbf{x}}_n, f(\mathbf{x}_n))\}$
- 10: **end for**
- 11: **return** $\text{BASELINEHPI}(\tilde{\mathcal{D}}, d)$

E Supplementary Analysis for the Ablation Study Using Standard Local HPI

E.1 Leakage of Gating Effects in Standard Local HPI

Let $b_{\gamma'} := \mathbf{1}\{\mathbf{x} \in \mathcal{X}_{\gamma'}\}$ be the top-set indicator. Consider a *gating* hyperparameter $x^{(c)}$ and a *conditional (child)* hyperparameter $x^{(d)}$ whose regime is determined by $x^{(c)}$. Formally, assume that for a conditional hyperparameter $x^{(d)}$ there exists a measurable mapping $\phi^{(d)} : \mathcal{X}^{(c)} \rightarrow \{1, \dots, K^{(d)}\}$ such that:

$$I^{(d)} = \phi^{(d)}(x^{(c)}) \quad \text{a.s.}, \quad (17)$$

where $I^{(d)} \in \{1, \dots, K^{(d)}\}$ denotes the random variable representing the regime index of the d -th hyperparameter. Moreover, assume that $x^{(c)}$ affects $b_{\gamma'}$ only through the induced regime (i.e., $x^{(c)}$ has no within-regime effect):

$$\mathbb{E}_{\gamma} [b_{\gamma'} \mid x^{(c)}] = \mathbb{E}_{\gamma} [b_{\gamma'} \mid I^{(d)}] \quad \text{a.s.}, \quad (18)$$

where the expectations are taken under the empirical distribution restricted to the top- γ region \mathcal{X}_{γ} .

Here, $x^{(c)}$ corresponds to the gating variable c in the synthetic objectives (Equations (6) and (9)), while $x^{(d)}$ corresponds to the

conditional variables x and y . These assumptions are satisfied by the synthetic objectives used in our experiments.

Then, we have the following result regarding the standard local HPI of the conditional hyperparameter $x^{(d)}$.

THEOREM E.1 (LEAKAGE OF GATING EFFECTS UNDER THE STANDARD LOCAL HPI). *Under the above assumptions (Equations (17) and (18)), the standard local marginal variance of the conditional hyperparameter $x^{(d)}$ contains the local marginal variance of the gating hyperparameter $x^{(c)}$:*

$$v_Y^{(d)} = v_{Y,\text{within}}^{(d)} + v_Y^{(c)}. \quad (19)$$

In particular, $v_Y^{(c)} \leq v_Y^{(d)}$.

The proof is provided in Appendix E.2. Consequently, when HPI is computed from $v_Y^{(d)}$, the effect of the gating variable $x^{(c)}$ is additively inherited by conditional hyperparameters through the inter-regime term.

This theorem is consistent with our empirical observations. In Figure 3, when using the standard local HPI, the importance of the gating variable c is always no larger than those of x and y . Moreover, in the regions of γ' where x or y is inactive, their HPI becomes almost identical to that of c . This is exactly what Theorem E.1 predicts: once $v_{Y,\text{within}}^{(d)}$ vanishes for an inactive variable, the standard local variance $v_Y^{(d)}$ reduces to the additive gating term $v_Y^{(c)}$.

E.2 Proof of Theorem E.1

PROOF. In this section, all expectations and variances are taken under the empirical distribution restricted to the top- γ region \mathcal{X}_Y , and we omit the subscript γ on \mathbb{E} and Var for notational simplicity.

Recall we defined $g_Y^{(d)}(I^{(d)}, Z^{(d)}) := \mathbb{E}[b_{Y'} | I^{(d)}, Z^{(d)}]$ in Section 4.2. We also restate the variance decomposition in Equation (2) here for convenience:

$$\begin{aligned} v_Y^{(d)} &= \text{Var}_{I^{(d)}, Z^{(d)}} \left(g_Y^{(d)}(I^{(d)}, Z^{(d)}) \right) \\ &= \underbrace{\mathbb{E}_{I^{(d)}} \left[\text{Var}_{Z^{(d)}} \left(g_Y^{(d)}(I^{(d)}, Z^{(d)}) \middle| I^{(d)} \right) \right]}_{\text{within-regime variance: } v_{Y,\text{within}}^{(d)}} \\ &\quad + \underbrace{\text{Var}_{I^{(d)}} \left(\mathbb{E}_{Z^{(d)}} \left[g_Y^{(d)}(I^{(d)}, Z^{(d)}) \middle| I^{(d)} \right] \right)}_{\text{inter-regime variance}}. \end{aligned} \quad (20)$$

By the tower property, we have:

$$\begin{aligned} \mathbb{E}_{Z^{(d)}} \left[g_Y^{(d)}(I^{(d)}, Z^{(d)}) \middle| I^{(d)} \right] &= \mathbb{E}_{Z^{(d)}} \left[\mathbb{E}[b_{Y'} | I^{(d)}, Z^{(d)}] \middle| I^{(d)} \right] \\ &= \mathbb{E}[b_{Y'} | I^{(d)}]. \end{aligned}$$

Thus, the inter-regime variance in Equation (20) equals:

$$\begin{aligned} v_{Y,\text{inter}}^{(d)} &:= \text{Var}_{I^{(d)}} \left(\mathbb{E}_{Z^{(d)}} \left[g_Y^{(d)}(I^{(d)}, Z^{(d)}) \middle| I^{(d)} \right] \right) \\ &= \text{Var}_{I^{(d)}} \left(\mathbb{E}[b_{Y'} | I^{(d)}] \right). \end{aligned} \quad (21)$$

On the other hand, the local marginal mean of the top-set indicator $b_{Y'}$ with respect to the gating coordinate $x^{(c)}$ is:

$$\begin{aligned} f_Y^{(c)}(x^{(c)}) &:= \frac{1}{Z_Y^{(c)}(x^{(c)})} \sum_{n=1}^N b_{Y'}(x^{(c)}, x_n^{(c)}) b_Y(x^{(c)}, x_n^{(c)}), \\ &= \mathbb{E}[b_{Y'} | x^{(c)}]. \end{aligned}$$

Thus, by Equation (18), we have:

$$\begin{aligned} v_Y^{(c)} &:= \text{Var}_{x^{(c)}} \left(f_Y^{(c)}(x^{(c)}) \right) \\ &= \text{Var}_{x^{(c)}} \left(\mathbb{E}[b_{Y'} | x^{(c)}] \right) \\ &= \text{Var}_{x^{(c)}} \left(\mathbb{E}[b_{Y'} | I^{(d)}] \right). \end{aligned} \quad (22)$$

From Equation (17), the quantity $\mathbb{E}[b_{Y'} | I^{(d)}]$ is a function of $x^{(c)}$ through $I^{(d)}$. Therefore,

$$\text{Var}_{x^{(c)}} \left(\mathbb{E}[b_{Y'} | I^{(d)}] \right) = \text{Var}_{I^{(d)}} \left(\mathbb{E}[b_{Y'} | I^{(d)}] \right). \quad (23)$$

Comparing Equations (21) to (23), we conclude that the inter-regime variance of the conditional hyperparameter $x^{(d)}$ equals the marginal variance of the gating hyperparameter $x^{(c)}$:

$$v_{Y,\text{inter}}^{(d)} = v_Y^{(c)}.$$

Substituting this into Equation (20) completes the proof. \square

E.3 Decomposition of PED over Regimes

Here, we use the notation defined in Appendices B.1 and B.2. That is, on the extended domain $S^{(d)}$, $\mu_Y^{(d)}$ and $\mu_{Y'}^{(d)}$ denote the empirical distributions of the extended d -th hyperparameter induced by the samples in \mathcal{X}_Y and $\mathcal{X}_{Y'}$, respectively.

We can then show the following decomposition of the Pearson divergence between $\mu_Y^{(d)}$ and $\mu_{Y'}^{(d)}$ on $S^{(d)}$.

LEMMA E.2 (REGIME-WISE DECOMPOSITION OF PEARSON DIVERGENCE). *Assume $\mu_{Y'}^{(d)} \ll \mu_Y^{(d)}$ and $\mu_{Y',i}^{(d)} \ll \mu_{Y,i}^{(d)}$ for every i with $\beta_i^{(d)} > 0$. Then the Pearson divergence between the extended marginals satisfies:*

$$\begin{aligned} D_{\text{PE}} \left(\mu_{Y'}^{(d)} \middle\| \mu_Y^{(d)} \right) &= \underbrace{\sum_{i=1}^{K^{(d)}} \frac{(\alpha_i^{(d)})^2}{\beta_i^{(d)}} D_{\text{PE}} \left(\mu_{Y',i}^{(d)} \middle\| \mu_{Y,i}^{(d)} \right)}_{\text{within-regime divergence}} \\ &\quad + \underbrace{D_{\text{PE}} \left(\alpha^{(d)} \middle\| \beta^{(d)} \right)}_{\text{inter-regime divergence}} \end{aligned} \quad (24)$$

where $\alpha^{(d)} := (\alpha_i^{(d)})_{i=1}^{K^{(d)}}$ and $\beta^{(d)} := (\beta_i^{(d)})_{i=1}^{K^{(d)}}$ are the discrete distributions over regimes.

The proof is provided in Appendix E.4. The absolute continuity $\mu_{Y'}^{(d)} \ll \mu_Y^{(d)}$ holds for the extended marginals in the same way as in Equation (1). The regime-wise $\mu_{Y',i}^{(d)} \ll \mu_{Y,i}^{(d)}$ also holds for all regimes with $\beta_i^{(d)} > 0$, since absolute continuity is preserved under restriction to measurable subsets. If a regime i corresponds to an inactive configuration (i.e., $\mathcal{Z}_i^{(d)} = \{\perp\}$), then $\mu_{Y',i}^{(d)}$ and $\mu_{Y,i}^{(d)}$

are both degenerate at \perp , so $D_{\text{PE}}\left(\mu_{Y',i}^{(d)} \middle\| \mu_{Y,i}^{(d)}\right) = 0$ and only the inter-regime term contributes.

Using this decomposition, we obtain Equation (11).

E.4 Proof of Lemma E.2

PROOF. Here, we omit the superscript (d) for notational simplicity. Since $\mu_{Y'} \ll \mu_Y$ and $\mu_{Y',i} \ll \mu_{Y,i}$ holds for $\beta_i > 0$, the Radon–Nikodým derivative $d\mu_{Y'}/d\mu_Y$ exists and is given by:

$$\frac{d\mu_{Y'}}{d\mu_Y}(x) = \frac{d(\alpha_i \mu_{Y',i})}{d(\beta_i \mu_{Y,i})}(x) = \frac{\alpha_i}{\beta_i} \frac{d\mu_{Y',i}}{d\mu_{Y,i}}(x),$$

for $x \in A_i$. We denote $s_i := d\mu_{Y',i}/d\mu_{Y,i}$.

The Pearson divergence can be expressed as follows:

$$\begin{aligned} D_{\text{PE}}(\mu_{Y'} \parallel \mu_Y) &= \int \left(\frac{d\mu_{Y'}}{d\mu_Y} - 1 \right)^2 d\mu_Y \\ &= \sum_{i=1}^{K^{(d)}} \int_{A_i^{(d)}} \left(\frac{\alpha_i}{\beta_i} s_i - 1 \right)^2 d(\beta_i \mu_{Y,i}) \\ &= \sum_{i=1}^{K^{(d)}} \beta_i \int \left(\frac{\alpha_i}{\beta_i} s_i - 1 \right)^2 d\mu_{Y,i} \\ &= \sum_{i=1}^{K^{(d)}} \left(\frac{\alpha_i^2}{\beta_i} \int s_i^2 d\mu_{Y,i} - 2\alpha_i \int s_i d\mu_{Y,i} + \beta_i \right). \end{aligned} \tag{25}$$

Here, we have:

$$\int s_i d\mu_{Y,i} = \int \frac{d\mu_{Y',i}}{d\mu_{Y,i}} d\mu_{Y,i} = \mu_{Y',i}(A_i) = 1. \tag{26}$$

Thus, we obtain:

$$\begin{aligned} \int s_i^2 d\mu_{Y,i} &= \int s_i^2 d\mu_{Y,i} - 2 \int s_i d\mu_{Y,i} + 1 + 1 \\ &= \int (s_i - 1)^2 d\mu_{Y,i} + 1 \\ &= D_{\text{PE}}(\mu_{Y',i} \parallel \mu_{Y,i}) + 1. \end{aligned} \tag{27}$$

By substituting Equations (26) and (27) into Equation (25), we have:

$$\begin{aligned} D_{\text{PE}}(\mu_{Y'} \parallel \mu_Y) &= \sum_{i=1}^{K^{(d)}} \left(\frac{\alpha_i^2}{\beta_i} (D_{\text{PE}}(\mu_{Y',i} \parallel \mu_{Y,i}) + 1) - 2\alpha_i + \beta_i \right) \\ &= \sum_{i=1}^{K^{(d)}} \left(\frac{\alpha_i^2}{\beta_i} D_{\text{PE}}(\mu_{Y',i} \parallel \mu_{Y,i}) + \frac{(\alpha_i - \beta_i)^2}{\beta_i} \right) \\ &= \sum_{i=1}^{K^{(d)}} \frac{\alpha_i^2}{\beta_i} D_{\text{PE}}(\mu_{Y',i} \parallel \mu_{Y,i}) + \sum_{i=1}^{K^{(d)}} \frac{(\alpha_i - \beta_i)^2}{\beta_i} \\ &= \sum_{i=1}^{K^{(d)}} \frac{\alpha_i^2}{\beta_i} D_{\text{PE}}(\mu_{Y',i} \parallel \mu_{Y,i}) + D_{\text{PE}}(\alpha \parallel \beta). \end{aligned}$$

This completes the proof. \square